Czech Technical University in Prague

Faculty of Electrical Engineering
Department of Radio Engineering

Master's thesis

Bearing Fault Detection in Nonstationary Operating Conditions

Detekce poruch ložisek při proměnných otáčkách

Author: Bc. Adam Kubíček
Supervisor: prof. Ing. Pavel Sovka, CSc.

May 2021

ZADÁNÍ DIPLOMOVÉ PRÁCE

I. OSOBNÍ A STUDIJNÍ ÚDAJE

Příjmení: **Kubíček** Jméno: **Adam** Osobní číslo: **434777**

Fakulta/ústav: **Fakulta elektrotechnická**

Zadávající katedra/ústav: **Katedra radioelektroniky**

Studijní program: **Elektronika a komunikace**

Specializace: **Audiovizuální technika a zpracování signálů**

II. ÚDAJE K DIPLOMOVÉ PRÁCI

Název diplomové práce:

Detekce poruch ložisek při proměnných otáčkách

Název diplomové práce anglicky:

Bearing Fault Detection in Nonstationary Operating Conditions

Pokyny pro vypracování:

1. Prostudujte problematiku analýzy vibrací se zaměřením na detekci vad ložisek, typů závad a určení jejich frekvencí v závislosti na otáčkové frekvenci.
2. Analýzou dostupných databází určete potřebné parametry a navrhněte vhodný algoritmus pro generování modelových nestacionárních signálů typických závad ložisek. Vytvořte příslušnou databázi signálů a proveďte její popis pro účely experimentů
3. Pomocí signálů databáze proveďte analýzy pomocí spektrogramu, přičemž pro výběr optimálních parametrů spektrogramu použijte metodu kurtogramu. Posuďte schopnost spektrogramu izolovat děje odpovídající příslušné vadě ložiska
4. Výsledky analýzy nestacionárních signálů databáze získané pomocí spektrogramu porovnejte s výsledky dosažitelné pomocí modifikace spektrogramu metodou označovanou jako synchrosqueezing Fourier based transform

Seznam doporučené literatury:

[1] Randall, R. B. a Antoni, J.: Rolling Element Bearing Diagnostics - A tutorial. Mechanical Systems and Signal Processing, 2011, 25 (2), s. 485–520
[2] Auger F. et al.: Time-Frequency Reassignment and Synchrosqueezing: An overview. IEEE Signal Processing Magazine, 2013, 30 (6), s. 32-41.

Jméno a pracoviště vedoucí(ho) diplomové práce:

prof. Ing. Pavel Sovka, CSc., katedra teorie obvodů FEL

Jméno a pracoviště druhé(ho) vedoucí(ho) nebo konzultanta(ky) diplomové práce:

Datum zadání diplomové práce: **29.01.2021** Termín odevzdání diplomové práce: **21.05.2021**

Platnost zadání diplomové práce: **30.09.2022**

prof. Ing. Pavel Sovka, CSc. podpis vedoucí(ho) práce	doc. Ing. Josef Dobeš, CSc. podpis vedoucí(ho) ústavu/katedry	prof. Mgr. Petr Páta, Ph.D. podpis děkana(ky)

III. PŘEVZETÍ ZADÁNÍ

Diplomant bere na vědomí, že je povinen vypracovat diplomovou práci samostatně, bez cizí pomoci, s výjimkou poskytnutých konzultací. Seznam použité literatury, jiných pramenů a jmen konzultantů je třeba uvést v diplomové práci.

. Datum převzetí zadání

Podpis studenta

Declaration of originality

I, the undersigned, hereby declare that I have developed the diploma thesis "Bearing Fault Detection in Nonstationary Operating Conditions" on my own and that the statement of resources presented in this work is a complete statement of all resources used.

In Prague on signature

Acknowledgement

I would like to express my deepest gratitude to my master's thesis supervisor, prof. Ing. Pavel Sovka, CSc. who introduced me to the subject of digital signal processing and supervised my diploma thesis. His remarkable supportive leadership during this master's thesis was inspiring in many ways. Furthermore, I would like to thank my parents and sister, who have always supported and motivated me during my university studies.

This work is dedicated to my beloved father, Ing. Pavel Kubíček, who sadly passed away in time when this work was in the making.

Abstract

This master's thesis deals with the fault diagnostics of rolling element bearing — namely types of faults and determination of the fault frequency known as ball pass frequency (BPF). Furthermore, the nonstationary bearing fault signals database was created for experimental purposes. This database is based on the required parameters. Such parameters were obtained by analyzing real bearing fault signals. The frequency analysis using Short-time Fourier transform, which time-related output is well known as the Spectrogram, has been done with generated signals from the created database. For the purposes of determining the parameters of the Spectrogram, a method called Kurtogram was used. The outputs of the frequency analysis using Spectrogram were compared to the outputs of the frequency analysis method known as the Fourier-based Synchrosqueezing Transform.

Keywords: Rolling element bearing, nonstationary, signal, fault, database, ballpass frequency, spectrogram, kurtogram, Fourier-based Synchrosqueezing Transform

Abstrakt

Tato diplomová práce se zabývá diagnostikou poruch valivých ložisek - konkrétně jednotlivými typy poruch a určováním frekvence poruch známou jako ballpass frekvence (BPF). Dále byla pro experimentální účely vytvořena databáze nestacionárních signálů vad ložisek. Tato databáze je založena na požadovaných parametrech reálných signálů vad ložisek. Tyto parametry byly získány z analýzy reálných nestacionárních signálů. Frekvenční analýza pomocí krátkodobé Fourierovy transformace, jejíž časově závislý výstup je dobře známý jako spektrogram, byla provedena s vygenerovanými signály z vytvořené databáze. Pro účely stanovení parametrů spektrogramu byla použita metoda zvaná kurtogram. Výstupy frekvenční analýzy pomocí spektrogramu byly porovnány s výstupy metody frekvenční analýzy známé jako Fourier-based Synchrosqueezing Transform.

Klíčová slova: Ložisko, nestacionární, signál, porucha, databáze, ballpass frekvence, spektrogram, kurtogram, Fourier-based Synchrosqueezing Transform

Contents

List of Figures

List of Tables

Chapter 1

Introduction

Due to the fact that bearings are an indispensable machine part, it is also essential to monitor the condition of the bearing to prevent failure of part of a machine or even the entire machine system. This part of engineering industry is subject to a constant process of innovation in order to maximize the life cycle of a bearing.

Many types of wear are noted during the use of the bearing. Certain types of wear generate vibration pulses, which are detectable by sensors designed for a given type of detection. Based on this phenomenon, many methods have emerged to approach the evaluation of such scanned data in order to detect or specify the nature of the fault.

This work focused not only on fault detection but also on the generation of non-stationary signals containing certain types of bearing faults. Nonstationarity can be modeled by a non-constant speed of bearing rotation. The necessary parameters for generating fault bearing signals should be obtained from the analysis of real signals so that these generated outputs correspond to some extent to reality. For the purposes of experiments, it is appropriate to create a database of non-stationary bearing fault singals.

It is important to mention that this work was created at the same time as the work [5]. It is, therefore, possible that in some cases, the works overlap slightly, but throughout the elaboration, an effort was made to distinguish these works not only by the assignment but by the overall approach to the solution. It should also be mentioned that the author is aware that Chapter 4 contains both the theory of methods used and practical results. This approach is not common but has been used to maintain the continuity of ideas and the compactness of the work.

The whole work is divided into 6 chapters, where each chapter has its own subchapters for better orientation in the text.

In the introductory chapter, the reader is acquainted with the issue of bearing failures. After a slightly theoretical introduction, the most common types of bearing failures are ana-

lyzed. At the end of the chapter, important mathematical relationships for determining fault frequencies are mentioned.

The following chapter 3 describes the physical properties of the generated vibration pulses. The created signal generator generates non-stationary fault bearing signals with the occurrence of inner/outer race fault. The emergence of the Non-stationary Bearing Fault Signal Database is considered an important output of this chapter.

Chapter 4 describes in detail the created fault bearing detection process. The methods used are described. The parameter values used are based on analyzes and practical justifications.

In the penultimate chapter, a test of the signal analysis algorithm is performed on signals from the Non-stationary Bearing Fault Signal Database. The results lead to a comparison of the two methods used, namely spectrogram and fsstgram.

The last chapter summarizes the main findings of the work and discusses the possible expansion of the work in the future.

Chapter 2

Mechanical Bearings and Rolling Element Bearing Faults

A bearing is a machine element in which another part (such as a ball or a roller) turns or slides to reduce friction during the machine parts' mutual rotating or sliding movement. It also constrains relative motion to only the desired motion. For example, the bearing design may provide free linear movement of the moving part or free rotation about a fixed axis. The term "bearing" is derived from the verb "to bear" [6] - bearing being a machine element that allows one part to bear (i.e., to support) another.

It is considered one of the most widely used machine parts, and thus it is required to be fully functional within its life cycle. Their failure is one of the most frequent reasons for machine breakdown [3].

The invention of the rolling bearing dates back to antiquity, when wooden rollers were used for bearing an object while it was moved. Around 1500 AD Leonardo da Vinci described a type of ball bearing in his design for a helicopter. The first patent is issued for Timken Tapered roller bearings in 1898. The modern, self-aligning design of ball bearing is attributed to Sven Wingquist of the SKF ball-bearing manufacturer in 1907 [7].

2.1 Types of bearings

There are many types of bearings which can be used in a variety of application. The modern developement of bearings is focused on reducing friction, increase bearing load, increase momentum build-up, and speed.

The main types of bearings are:

- **Plain bearing** - the simplest type of bearing, which contains only the bearing surface and no rolling elements. It usually has a rubbing surface with lubricant;
- **Rolling element bearing** - a bearing which carries a load by placing rolling elements (such as balls or rollers) between two bearing rings called races;
  - **Ball bearing** - rolling elements are spherical balls;
  - **Roller bearing** - rolling elements are cylindrical, taper or spherical rollers;
- **Jewel bearing** - a plain bearing in which a metal spindle turns in a jewel-lined pivot hole. It is usually used in mechanical watches;
- **Fluid bearing** - a bearing in which the load is supported by a thin layer of rapidly moving pressurized liquid or gas between the bearing surfaces;
- **Magnetic bearing** - a type of bearing that supports a load using magnetic levitation;
- **Composite bearing** - plain bearing shape with PTFE liner on the interface between bearing and shaft with a laminated metal backing. PTFE acts as a lubricant.

According to the direction of the force applied, the bearings are divided into:

- **Radial** - perpendicular to the bearing tracks;
- **Axial** - longitudinally with bearing tracks [3].

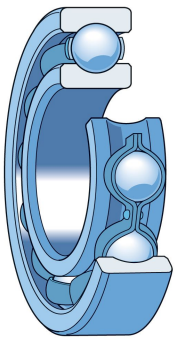

Figure 1: Rolling Element Bearing. The balls fit well into the deep grooves, enabling the bearing to support axial loads in both directions, in addition to radial loads. The bearing illustrated here has a single row of balls [1].

The level of friction is an important index of efficiency in bearings. By reducing friction, we want to reduce the level of weariness, to extended usage at high speeds, and to avoid overheating and premature failure of the bearing. This can be achieved by several factors such as:

- **Shape** - gains advantage usually by using balls or rollers;
- **Material** - each material has specific properties, and its usage depends on the method of application;
- **Fluid** - a low viscosity fluid such as lubricants is used to keep the two solid parts from touching;
- **Fields** - a magnetic field is used to keep the two solid parts from touching;
- **Air pressure** - air pressure is used a magnetic field is used to keep the two solid parts from touching.

Oil, grease, or solid lubricants are used for reducing friction[8]. A specific type of lubricant depends on the pressure of a load and the ambient temperature.

2.2 Rolling element bearing faults

As it was mentioned rolling element bearings are widely used machine elements. Thus, it is important to do maintenance tasks to prevent bearing failure or failure of the whole machinery system. Due to metal-to-metal contact, it is easy to wear out for rolling element bearings. That leads to failure of a specific part of the bearing, such as inner or outer race or rolling element. The bearing can fail for several reasons: inadequate lubrication (too much or too little lubricant), contaminated lubricant, overload, improper handling or assembly, sudden temperature changes, age (surface fatigue), external vibrations, manufacturing defects, or contamination by dirt particles [9].

Even the method of storage affects the proper functioning of the bearings. For example, the service life of bearings in one application was extended dramatically by changing how the bearings were stored before installation and use. Vibrations during storage caused lubricant failure even when the only load on the bearing was its weight [10, 11].

Despite operating correctly, rolling element bearings will eventually fail as a result of a surface fatigue phenomenon. Rolling element bearing surface fatigue is characterized by spalling. This failure is characterized as surface damage. After a while, the particles of the material start to break off. This creates cracks on the surface, which propagate into the material. As

the rolling elements pass through the cracks, material particles break off, contaminating the entire bearing system. Spalling leaves cavities at contact surfaces with a depth of 20 µm to 100 µm.

Another type of rolling bearing failure is so-called pitting. Due to the higher load than the roller bearing is designed, cracks are formed inside the material. These cracks propagate to the surface over time. As the rolling elements pass through the cracks, material particles break off, contaminating the entire bearing system. Pitting appears as shallow craters at contact surfaces with a depth of, at most, the thickness of the work-hardened layer (approximately l0 µm) [11].

Both of these types of faults produce acoustic/vibrating pulses that are detectable by, for example, a microphone or an accelerometer. Following proper analysis of these signals can identify the specific type of fault, which indicates what part of the bearing is damaged.

2.3 Vibrations

A mechanical motion that repeats itself after an interval of time is called vibration or oscillation. Vibration refers to mechanical oscillations about an equilibrium point (Figure 2). Vibrations usually are an undesirable element during the operation. They are wasting energy and creating an unwanted sound which is considered noise.

When the rolling elements of a bearing get in contact with the surface that is damaged, an impulse is generated. This type of vibration signal occurs periodically, producing a harmonic series with a fundamental frequency that depends on the material properties of the surface [9].

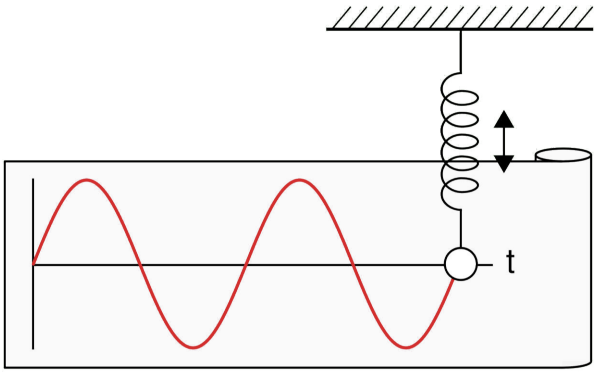

Figure 2: The vibration signal is visualized as a simple harmonic motion.

We recognize 3 types of vibrations:

- **Free vibration** is the oscillation of the system without the action of external forces, i.e., the system is set out of balance, released, and left in motion without excitation. The mechanical system vibrates at one or more of its natural frequencies and damps down to motionlessness.
- **Forced vibration** is when a time-varying disturbance (load, displacement or velocity) is applied to a mechanical system.
- **Damped vibration** occurs when the energy of a vibrating system is gradually dissipated by friction and other resistances; the vibrations are said to be damped. The vibrations gradually reduce or change in frequency or intensity and the system rests in its equilibrium position. Damped vibration is a type of vibration which occurs at rolling element bearing fault signals.

Sources of vibrations in Rotating Machine element are:

- Misalignment of couplings, bearings and gears,
- Unbalance of rotating components,
- Looseness,
- Degradation of rolling element bearings,
- Gear wear,
- Eccentricity of rotating components such as "v" belt pulleys or gears,
- Bent shaft,
- Resonance,
- Electrical problems in motors.[12]

2.4 Bearing fault frequencies

Due to the reasons mentioned in previous subchapters, every damaged rolling bearing generates vibrations during its operation in the machine. The vibration signal is converted to a digital signal by sensors (i.e., accelerometers) located on the bearing. In the signal, we are able to see pulses that are periodically repeated depending on the shaft frequency, fault location,

and geometry of a bearing. This frequency of occurrences of vibration pulses is called fault frequency. We distinguish four types of failures according to their location in the bearing as a fault of the inner or outer race, rolling element (ball or roller), or bearing cage.

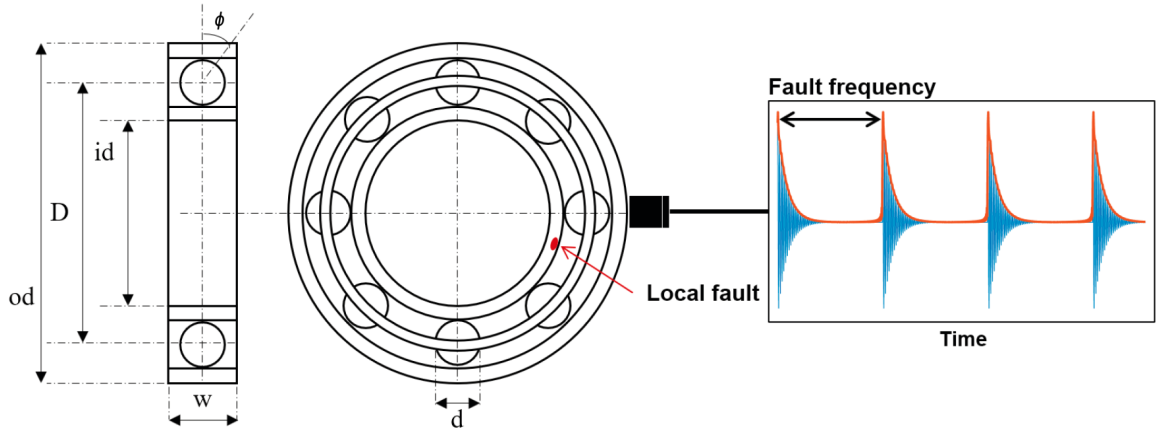

Figure 3: Rolling element bearing with localized inner race fault [2]. A vibration sensor is shown on the outside of the bearing. Subsequently, the course of these vibrations over time is also illustrated. od is the outter bearing diameter, D is the pitch diameter, id is the inner bearing diameter, ϕ is the bearing contact angle, and d is the ball diameter.

We are able to theoretically calculate fault frequencies that mean the rate of occurrences of the pulses generated by rolling elements passing over the place with a defect. These fault frequencies are generally masked in the low-frequency region due to the presence of deterministic components and noise from other components in the system, such as gears, blades, unbalance, misalignment, electrical noise, etc. The actual ball pass frequencies are generally 1-2 % in deviation from the theoretically calculated frequencies due to the slippage of the rolling elements as a result of the variation of the load angle [13, 3].

By the part of the bearing that is affected by the fault, we are able to determine four types of fault frequencies [3, 13]:

- **BPFO** - Ballpass frequency, outer race

$$BPFO = \frac{nf_r}{2}\left(1 - \frac{d}{D}cos\phi\right) \quad \text{[Hz]} \quad (2.1)$$

- **BPFI** - Ballpass frequency, inner race

$$BPFI = \frac{nf_r}{2}\left(1 + \frac{d}{D}cos\phi\right) \quad \text{[Hz]} \quad (2.2)$$

- **FTF** - Fundamental train frequency, also known as cage speed

$$FTF = \frac{f_r}{2}\left(1 - \frac{d}{D}cos\phi\right) \quad \text{[Hz]} \quad (2.3)$$

- **BSF/RSF** - Ball (roller) spin frequency

$$BSF = \frac{D}{2d}\left[1 - \left(\frac{d}{D}cos\phi\right)^2\right] \quad \text{[Hz]} \quad (2.4)$$

where *fr* is the shaft frequency speed, n is the number of rolling elements, d is the ball diameter (see Figure 3) , D is the pitch diameter (see Figure 3) , and ϕ is the angle of the load from the radial plane. In non-stationary operating conditions, the shaft speed *fr* varies over time.

It is good to be noted that the ball spin frequency (BSF) is the frequency with which the fault strikes the same race (inner or outer) so that in general, there are two pulses per basic period. Thus the even harmonics of BSF are often dominant, in particular in envelope spectra [3].

If the dimensions of the monitored bearings are not known, but only the number of rolling elements is known, it is possible to modify the formulas ((2.1) - (2.4)). However, this simplification results in a loss of calculation accuracy [8].

- **BPFO** - Ballpass frequency, outer race

$$BPFO = \left(\frac{n}{2} - 1,2\right)60f_r \quad \text{[Hz]} \quad (2.5)$$

- **BPFI** - Ballpass frequency, inner race

$$BPFI = \left(\frac{n}{2} + 1,2\right)60f_r \quad \text{[Hz]} \quad (2.6)$$

- **FTF** - Fundamental train frequency, also known as cage speed

$$FTF = \left(\frac{1}{2} - \frac{1,2}{n}\right)60f_r \quad \text{[Hz]} \quad (2.7)$$

- **BSF/RSF** - Ball (roller) spin frequency

$$BSF = \frac{n}{2}\left(\frac{n}{2} - 1,2\right)60f_r \quad \text{[Hz]} \quad (2.8)$$

As Figure 4 shows, there is a clearly visible presence of amplitude modulation in the inner race fault signal and rolling element fault signal. The frequency of the modulation signal is equal to the shaft rotation frequency *fr*. On the other hand, the outer race fault signal is not amplitude modulated at all. Such phenomenon will be discussed further in the next chapter. This trend is well seen from the envelope signal.

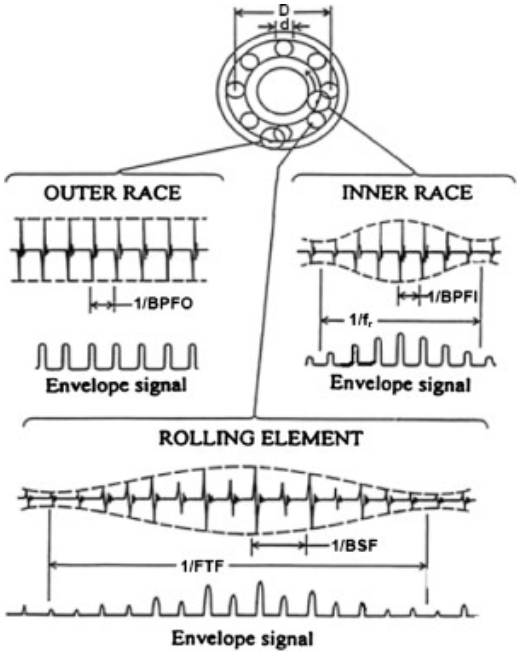

Figure 4: Typical signals and envelope signals from local faults in rolling element bearings [3].

Chapter 3

Generating Fault Signals

3.1 Fault Signal Generator

As mentioned in the previous chapter, bearing failures generate vibrational pulses. These pulses can be understood as a simplified model of damped oscillations. An important characteristic of these oscillations is that the frequencies of the bearing fault signals are distributed in the low-frequency band as well as in the high-frequency band. In the low-frequency band ($f < 1000$ Hz), the fault frequencies are present. On the other hand, the high-frequency band ($f = 1000 \sim 10000$ Hz) includes the frequency of the oscillation [13, 14].

The whole model of the signal generator and subsequent analysis was approached as a discrete system. The Matlab® development environment was used as a tool for the implementation of all operations.

3.1.1 Damped Oscillation Model

According to [15], the model of damped oscillations is determined by a linear ordinary differential equation of the 2nd order

$$\ddot{y}(t) + 2\zeta\omega_0\dot{y}(t) + \omega_0^2 y(t) = u(t). \tag{3.1}$$

For normalization purposes, it is advantageous to use

$$\ddot{y}(t) + 2\zeta\omega_0\dot{y}(t) + \omega_0^2 y(t) = \omega_0^2 u(t), \tag{3.2}$$

where ζ is the relative damping of the system and ω_0 is the natural frequency of oscillations. We understand the signals generated by bearing defects as a model of underdamping system. For such a system is $\zeta < 1$. And the solution of the characteristic equation has two complex conjugate roots

$$s_{1,2} = \sigma_p \pm j\omega_p, \tag{3.3}$$

where ω_p is the frequency of damped oscillations and $\sigma_p < 0$ is the damping of these oscillations.

For the underdamping system is $\omega_0 > \sigma_p$, and therefore the system oscillates with damped oscillations of ω_p frequency with exponential decreasing amplitude. Such a system is defined by a transfer function such as

$$h(t) = \frac{\omega_0}{\sqrt{1-\zeta^2}} e^{\sigma_p t} sin(\omega_p t) \tag{3.4}$$

for $t > 0$.

Due to the lack of suitable databases with the necessary non-stationary signals for this work's purposes, only one available database has been chosen with non-stationary signals - "Bearing vibration data collected under time-varying rotational speed conditions" [16]. Unfortunately, the data from this database was contaminated by severe noise, so it was not possible to determine all the necessary parameters. The parameter that could be determined using the kurtogram method was the impulse resonance frequency $f_c = \frac{\omega_p}{2\pi}$ [Hz].

The time constant $\tau = -\frac{1}{\sigma_p}$ [s] was determined in cooperation with the author of the work [5]. This parameter was determined by analyzing the "Condition Based Maintenance Fault Database for Testing of Diagnostic and Prognostics Algorithms" by MFPT [17]. These two values were set as constants with the following values:

- $f_c = 8000$ Hz,
- $\tau = 0.0005$ s.

The parameter τ was chosen as a constant because, in case of its variation of its value, the pulses could overlap at high-frequency shaft speeds. The same parameters were used in [13] as well. This work primarily focuses on the creation of non-stationary signal database and subsequent analysis algorithm.

After the determination of the constants f_c and τ, we can perform subsequent mathematical operations to calculate the remaining parameters of the system transfer function. Thus we can perform

$$\omega_p = 2\pi f_c \quad \text{[rad/s]} \tag{3.5}$$

$$\sigma_p = -\frac{1}{\tau} \quad \text{[rad/s]} \tag{3.6}$$

where ω_p is the impulse angular frequency. The natural frequency of oscillations ω_0 is determined by calculating the Pythagorean theorem

$$\omega_0 = \sqrt{\omega_p^2 + \sigma_p^2} \qquad [\text{rad/s}] \quad (3.7)$$

The last parameter to determine is the damping ratio ζ, which we obtain by the following equation.

$$\zeta = \frac{\sigma_p}{\omega_0} \qquad [\text{-}] \quad (3.8)$$

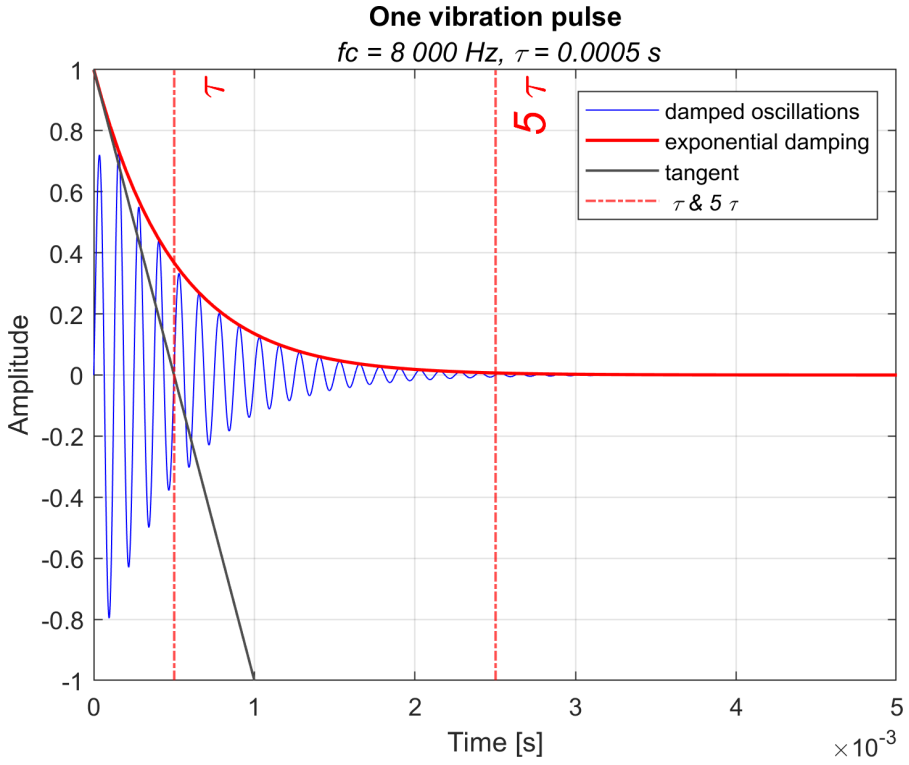

Figure 5: Modeling of one damped pulse.

Figure 5 shows the model of damed oscillation. The time constant τ is equal to the intersection of the x-axis and the tangent to the exponential damping. The value of 5τ is shown here to illustrate the 99.33 % decrease of the system vibrations. This value is important for determining the pulse length to ensure that the pulses do not interfere with each other at variable shaft frequency speeds.

3.1.2 Non-stationary operating conditions

Signal modeling under non-stationary conditions was performed by changing the shaft speed fr over time. This phenomenon resulted in a time change of the fundamental frequencies of the fault (see equations 2.1 - 2.4). In addition, this resulted in different spacing between pulses. In this work, a faulty bearing under ramp-down speed was constructed. A speed-down scenario is characterized by decreasing shaft speed and pulses amplitude over time. The algorithm for generating such a signal is described by the following equation

$$s(t) = \sum_{m=1}^{N} A_m e^{-\frac{t}{\tau}} \sin(2\pi f_c t) \tag{3.9}$$

where N is the signal length, $t\epsilon\langle 0, T_0\rangle$ where $T_0 = \frac{1}{BPF}$, where BPF is the fundamental frequency of a specific fault type (see equations (2.1) - (2.4)) which depends on the change of the shaft frequency fr. Decreasing amplitude A_m over time for the speed-down case is defined as

$$A_m = A\left(\frac{N}{f_s} - \eta t_m\right) \tag{3.10}$$

where A and η are constants. A defines the amplitude factor of the first pulse and is equal to $A = \frac{1}{T}$ where $T = \frac{N}{f_s}$. η defines the factor by how much the amplitude of the last pulse decreases compared to the first pulse amplitude ($0 \leq \eta \leq 1$) [18]. f_s is the sampling frequency and t_m is the occurence time of the mth impulse ($m = 1, 2, ...$) which should meet the condition $t_m \leq T$.

Typical values that were used in the simulation:

Constant	**Value**	**Units**	**Meaning**
f_c	8000	Hz	impulse resonance frequency
f_s	20000	Hz	sampling frequency
τ	0.0005	s	time costnatn
η	0.3	-	amplitude decreasing factor

Table 3.1: Table of constants used in generating non-stationary signals.

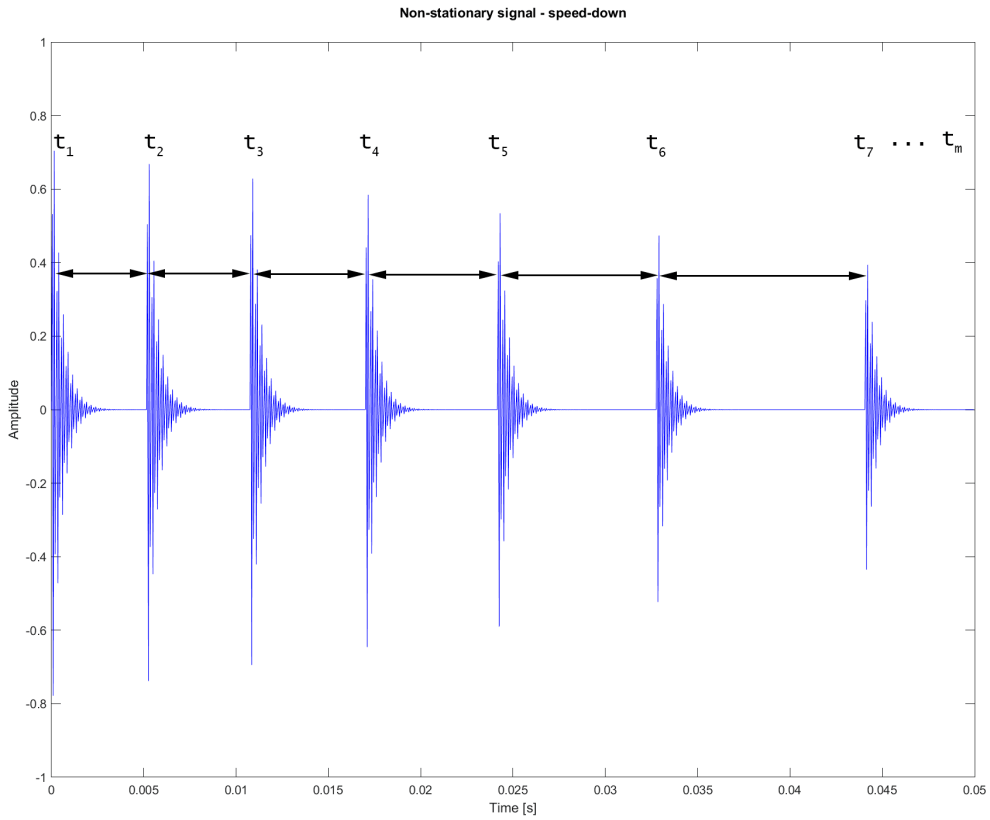

Figure 6: Simulated non-stationary signal under time-varying speed-down shaft speed.

3.2 Inner race fault

In most cases, the inner ring of the bearing is firmly connected to the rotating shaft. The vibration sensor is located on the outer ring of the bearing (see Figure 3), which is fixed. Due to this constellation, when the inner ring of the bearing rotates relative to the sensor, the resulting signal is amplitude modulated by the shaft rotation frequency f_r [9].

The frequency of pulses occurrences depends on the time-varying fundamental frequency BPFI (see equation (2.2)).

In the case of linearly time-varying shaft rotation frequency f_r, it is suitable to use a **linear chirp signal** as the modulation signal. The instantaneous frequency $f(t)$ of linear chirp is defined as follows

$$f(t) = ct + f_0 \tag{3.11}$$

where f_0 is the starting frequency ($t = 0$) and c is the chirp rate equal to

$$c = \frac{f_1 - f_0}{T} \tag{3.12}$$

where f_1 is the final frequency ($t = \frac{N}{f_s}$), T is the time required to sweep from f_0 to f_1.

The modulation signal as a time-domain function for a sinusoidal linear chirp is described as

$$m(t) = M \sin\left[\phi_0 + 2\pi\left(\frac{c}{2}t^2 + f_0 t\right)\right] \tag{3.13}$$

where M is the amplitude of modulation, ϕ_0 is the initial phase ($t = 0$) [19].

Subsequent **amplitude modulation** is given by mathematical equation

$$y(t) = [1 + m_i m(t)]s(t) \tag{3.14}$$

where m_i is the modulation index $m_i = \frac{M}{A_m}$ [20].

$m_i = 0.95$ was used in the next picture (Figure 7) and signal generator.

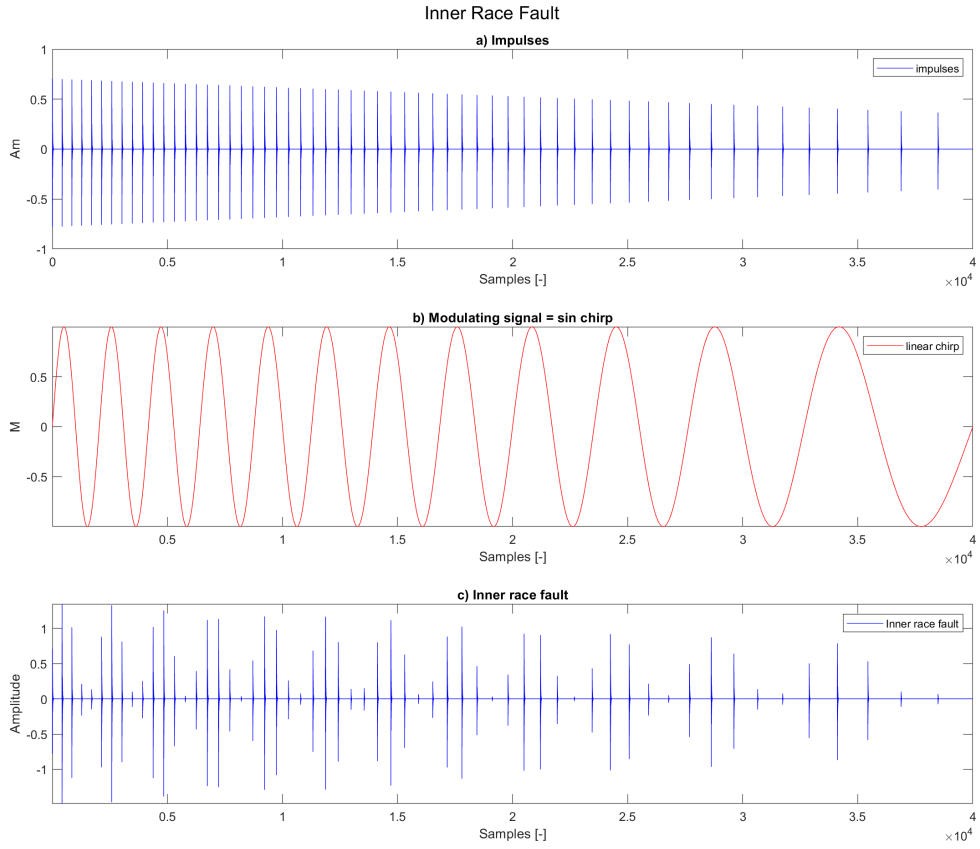

Figure 7: Generating Inner race fault. a) s(t) = sequence of impulses, b) m(t) = modulating signal (linear sine chirp), c) y(t) = generated inner race fault.

3.3 Outer race fault

Due to the location of the vibration sensor on the outside of the bearing, which does not move, no amplitude modulation is present in the outer race fault signal. This makes generating a signal of this type of error more simple than in the case of the inner race fault.

The frequency of pulses occurrences depends on the time-varying fundamental frequency BPFO (see equation 2.1).

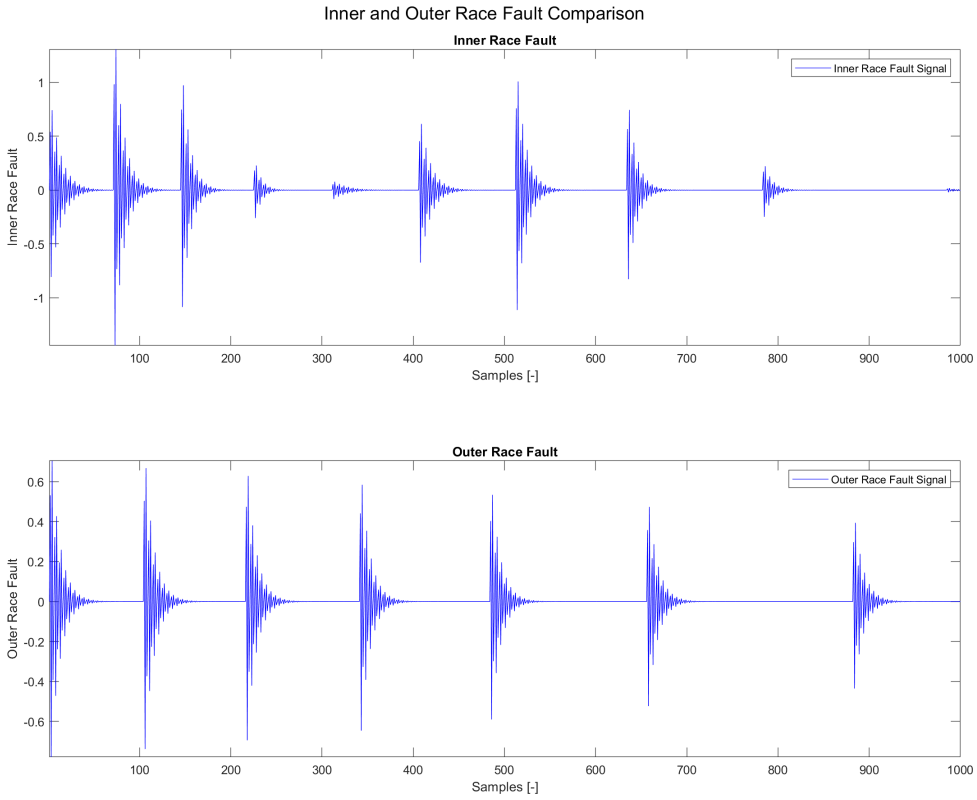

Figure 8: Comparison between Inner Race Fault signal (top) and Outer Race Fault signal (bottom).

The figure 8 illustrates that the signals do not only differ in the presence of amplitude modulation but also in the fundamental frequency value that depends on the fault type (see equations (2.1) and (2.2)). For both signals, the time change of the shaft speed frequency f_r is the same.

3.4 Jitter, deterministic components and additive noise

Due to the smearing effect of the rolling ball element are theoretically calculated fundamental frequencies $1 - 2\%$ in deviation from the actual fundamental ball pass frequencies. This phenomenon is called **jitter** [21].

The information about fundamental frequency is located in the low-frequency band. However, there are also present deterministic components and noise in this band that mask this information. Such interferences come from other components in the system such as gears, blades, unbalance, misalignment, electrical noise, etc [13].

Deterministic components were generated as two linear chirps. One with the same frequency change as the shaft speed frequency f_r and the second with double the time-varying shaft frequency speed with half the amplitude of the first chirp deterministic component.

Additive noise was generated as Additive white Gaussian noise (AWGN) with defined signal-to-noise ratio (SNR), which indicates the degree of noise presence in the signal [13].

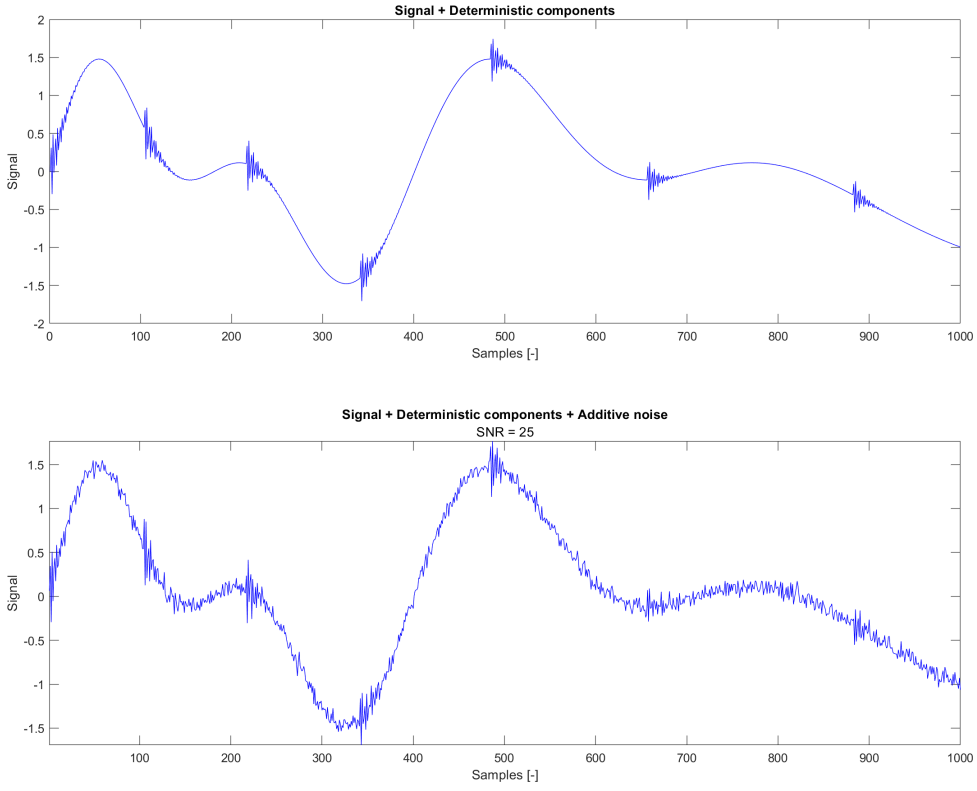

Figure 9: Illustrating of a signal contaminated by two deterministic components and additive noise with defined signal-to-noise ratio (in the figure: $SNR = 25$ dB).

3.5 Non-stationary Bearing Fault Signal Database

This chapter deals with the created databases of non-stationary bearing fault signals. All signals were generated using the signal generator discussed in the previous chapters 3.1 - 3.4.

The database was designed primarily for the purpose of capturing the non-stationary course of the bearing failure signal. For this reason, more bearing types were not considered. A shaft speed deceleration scenario was considered to capture non-stationarities in the signals. Two described faults were selected - namely Inner race fault and Outer race fault. Another important variable was the Signal-to-Noise Ratio (SNR) parameter. All generated signals have a duration of 3 seconds.

At the end of this chapter, a table with characteristic parameters of signals from the created database of non-stationary bearing fault signals is displayed.

3.5.1 Bearing type

The used bearing type is the same as in the described stationary database [17]. It is a ball bearing from the Nice Ball Bearings company, which has the following parameters:

- ball diameter $d = 0.5969$ cm,
- pitch diameter $D = 3.1623$ cm,
- number of rolling elements $n = 8$,
- contact angle $\phi = 0$.

These listed bearing parameters are necessary for the calculation of the fault frequencies (see equations (2.1)-(2.4)).

3.5.2 Shaft speed frequency

Non-stationary conditions were modeled by changing the value of the shaft speed f_r over time. The change of the frequency value is given by the parameters f_{start} and f_{stop}, which define the initial and final value of the change of the shaft speed frequency f_r.

The suitability of choosing the value f_{start} depends on the fact that the resulting fault frequency of the given fault type is not such that the pulses already interfere with each other. Therefore, the limit value of f_{start} was selected, which was set to 40 Hz. This value is based on the high-frequency speed of the Ingenuity helicopter, which took off on Mars on February 18, 2021, with a rate of 2400 RPM [22]. At this value, the condition of non-overlapping pulses for both types of faults is fulfilled.

f_{start} takes values of 40, 30 and 20 Hz and f_{stop} takes values of 15, 10 and 5 Hz.

3.5.3 Signal-to-noise ratio

The range of SNR values is from 60 to 20 dB. For SNR values less than 20 dB, the kurtogram method in signal analysis failed due to the presence of strong additive noise.

3.5.4 Output file naming system

For easy organization and orientation for users, the following system for determining the name of individual sets of non-stationary bearing fault signals has been introduced. The name format of the signal generator output signals is as follows:

`faultType_fstart_fstop_T_SNR.mat.`

where `faultType` is the type of bearing fault such as Inner/Outer race fault, `fstart` defines the initial frequency of the shaft speed f_r in Hz, `fstop` defines the frequency of the shaft speed f_r at the end of the signal, `T` is the duration of the signal in seconds and `SNR` defines the SNR value in dB.

Let's have a representative signal with the following parameters:

- fault type = Outer race fault,
- $f_{start} = 30$ Hz,
- $f_{stop} = 15$ Hz,
- $T = 3$ s,
- $SNR = 30$ dB.

Then, the output signal of the signal generator will be named in the following form.

`OUTER_30Hz_15Hz_3s_30.mat`

3.5.5 Meaning of variables in the output structure

The following table 3.2 describes the meaning of the individual variables, which are stored in the output structure of the file with the `*.mat` extension.

Name of the variable	**Meaning**
xw_out	bearing fault signal with deterministic components and additive noise
fs	sampling frequency [Hz]
fstart	initial shaft speed frequency [Hz]
fstop	final shaft speed frequency [Hz]
BPFM	time evolution of the fault frequency during the whole signal
BPFIM	time evolution of the theoretically calculated fault frequency of the Inner race fault type [Hz]
BPFOM	time evolution of the theoretically calculated fault frequency of the Outer race fault type [Hz]
frM	time evolution of the shaft speed frequency [Hz]
NiM	time evolution of the period length between pulse [samples]
poziceM	time occurrences of the pulses [samples]

Table 3.2: A table describing the meaning of the individual variables stored in the output file of the signal generator.

3.5.6 Generated signals and their key properties

The following tables (6.1 and 6.2) located in the attachment section describes the generated signal database with the basic descriptive parameters of the signals.

Chapter 4

Signal Analysis

Signal analysis or digital signal processing is a field of electronic engineering dealing with analyzing, modifying, or synthesizing signals such as audio, video, or in the case of this work - vibration signals. The roots of this scientific field are dated to the 17th century.

This chapter describes the idea of suggested analysis resulting in the algorithm to analyze the generated non-stationary linear speed-down vibration signals of the bearing faults (namely inner race fault and outer race fault). Since the field of analysis of non-stationary bearing fault signals has the potential to be more explored, the implemented solution in this work is ready for further possible modifications to improve the results.

The following block diagram (Figure 10) outlines the analysis procedure. The implemented algorithm contains several specific methods, which will be described in more detail below, and their outputs will be presented. Two main approaches were used in the analysis using:

- Short-time Fourier transform [23],
- Fourier Synchrosqueezed transform [24].

The ability of these two methods to solve the problem of fault detection is compared and discussed. At the end of this chapter, a solution is outlined that goes beyond the limits of this algorithm and attempts to detect the fault type. It is important to emphasize that the scope of this work primarily seeks to detect a bearing fault, not to classify it. But the potential of the generated data was used. Thus, not only the fault type is determined, but also the development of the pulse period and the subsequent development of the shaft frequency speed is determined.

The Matlab® development environment was used as a tool for the implementation of the whole analysis.

4.1 Block diagram

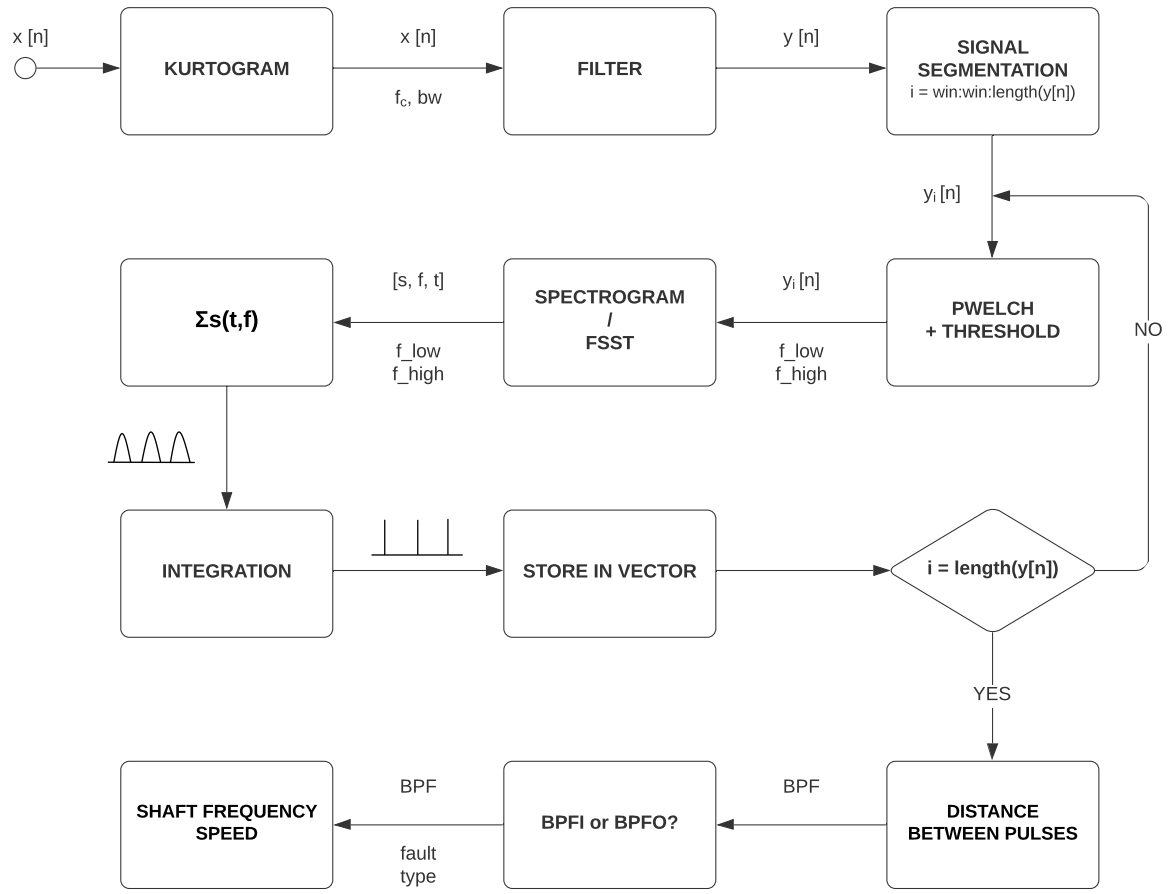

Figure 10: Block diagram describing the signal analysis algorithm for bearing fault detection. $x[n]$ is the input signal, f_c is the central frequency of the oscillations, bw is the bandwidth, $y[n]$ is the filtered signal, $y_i[n]$ is the i-th segment of $length = win$, f_{low} and f_{high} are the frequencies that define the band in which the spectrogram/fsstgram will be projected on the timeline, s, f, t are the output parameters of the spectrogram/fsstgram and BPF is the Ball pass frequency.

The input signal is filtered by a filter which parameters are determined by the output parameters of the Kurtogram method [25]. Subsequently, this signal is segmented, and in each segment of defined $length = win$, the Power spectral density (PSD) is calculated using the Welch's method [26]. The band in which the information about the vibration pulses is contained is determined using the given threshold level applied to PSD. The spectral values from this obtained band are then projected from the spectrogram/fsstgram to the time axis by

summing the frequencies in the given band at a given time. After performing this operation, we get a kind of envelope of vibrating pulses. We then integrate this signal from the given threshold level. These values are gradually stored in a vector, in which we can then determine the distance between the pulses, which indicates the value of the period $\frac{1}{BPF}$ [s]. From this point, we are able to determine the similarity of the values of the identified period with the theoretically calculated one using the given metric and thus determine the fault type. With the knowledge of fault type, we are able to modify the formula (equations (2.1) and (2.2)) in order to calculate the time-varying shaft speed frequency.

4.2 The Kurtogram

It is known from previous chapters that a damaged bearing generates vibrational pulses. These pulses have the characteristic property of high impulsivity. Therefore, it is possible to detect these pulses using appropriate methods even in the presence of additive noise.

It was recommended in the past to use the hammer tap testing to find bearing housing resonances [3]. But from the moment it is possible to use the method of spectral kurtosis or its two-dimensional representation kurtogram, we can analyze the data without reference values.

4.2.1 Spectral kurtosis

Spectral kurtosis provides the information on which frequency bands contain the maximum impulsivity signal. This method was first used in sonar systems in 1980s to detect impulsive events in sonar singlas [25]. The spectral kurtosis extends the concept of kurtosis. Kurtosis provides one global value about the impulsiveness of the signal and is defined as follows.

$$kurtosis = \frac{\frac{1}{N}\sum_{n=1}^{N}(x_n - \mu_x)^4}{\frac{1}{N}\sum_{n=1}^{N}((x_n - \mu_x)^2)^2} - 3 \tag{4.1}$$

where x is the analyzed signal, N is the number of samples of the signal x, μ_x is the mean value of the signal x. The subtraction of 3 is used to enforce $kurtosis = 0$ in the case x is real Gaussian.

On the other hand, the spectral kurtosis is the function of frequency and thus indicates how the impulsiveness of a signal, if any, is distributed in the frequency domain [3]. This method is derived from the Short-time Fourier transform method and thus it depends on the choice of the STFT window length. The spectral kurtosis is given by the following mathematical equation (equation 4.2).

$$K(f) = \frac{\langle |X(t,f)|^4 \rangle}{\langle |X(t,f)^2|^2 \rangle} - 2 \tag{4.2}$$

where $X(t,f)$ is the complex envelope of analyzed signal x. The subtraction of 2 is used to enforce $K(f) = 0$ in the case $X(t,f)$ is complex Gaussian [3].

4.2.2 The Kurtogram

Because the spectral kurtosis method is dependent on the definition of the STFT window length, it is appropriate to bring this dependence into a two-dimensional representation called the kurtogram. This can be understood as a cascade of spectral kurtosis values for different lengths of STFT windows (see Figure 11).

This function was called in the Matlab® development environment as follows:

```
[KGRAM, F, W, fc, wc, bw] = kurtogram(x,fs,level);
```

- `x` is the input signal with specific fault type,
- `fs` is the sampling frequency ($fs = 20000$ Hz),
- `level` determines the level of window resolution to use, and therefore how many spectral kurtosis cases to calculate ($level = 6$),
- `KGRAM` is the fast kurtogram of signal vector x represented as a matrix,
- `F` is the frequency vector for kurtogram,
- `W` is the window size vector for kurtogram,
- `fc` is frequency where the maximal spectral kurtosis is located,
- `wc` is window size where the maximal spectral kurtosis on the kurtogram is located,
- `bw` is suggested bandwidth for the optimal bandpass filter.

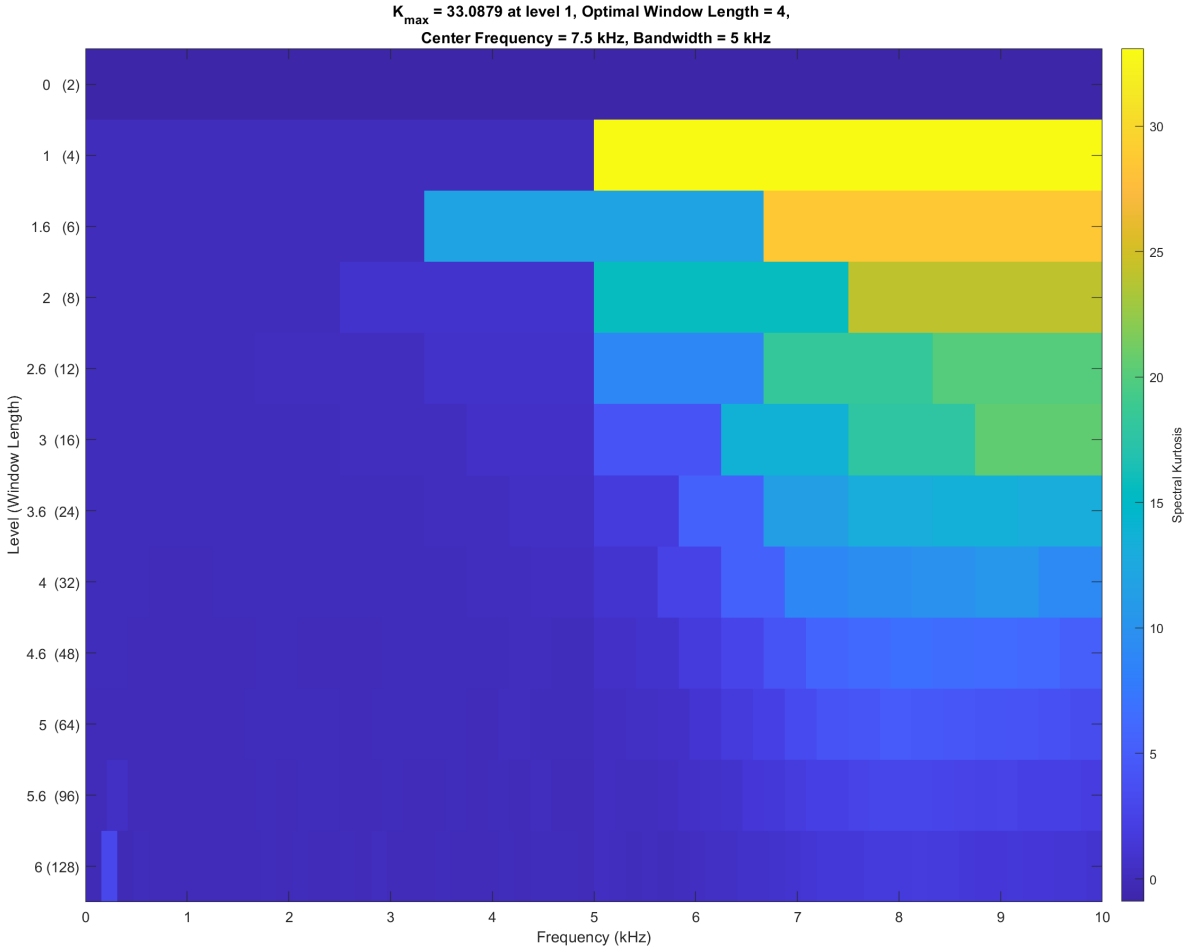

Figure 11: Illustration of the output of the kurtogram function in the Matlab® development environment. The warmer the color representation of the kurtogram, the higher the spectral kurtosis value for a given window length. Y-axis reffers to the length of the window and X-axis is the frequency axis.

Kurtogram method (see Figure 11) provides the key information such as central frequency f_c of a band, where the value of spectral kurtosis is the highest (K_{max}) for a given length of the STFT window. This center frequency should be around the center frequency of the oscillations. Another significant output parameter is the bandwidth bw. Thanks to these two parameters, we can successfully design a filter with which we can remove unwanted interference and thus obtain a useful signal of the non-stationary course of vibration pulses in time.

4.3 Filtration and Signal segmentation

4.3.1 Filtration

Electronic filters remove unwanted frequency components from the applied signal, enhance wanted ones, or both. In the case of this work, we want to remove deterministic components and suppress the effect of additive noise in order to obtain the useful signal of vibrational pulses. On the contrary, we want to avoid distortion of this useful signal.

After considering the possibilities of many types of approaches to filter design, it was based on the conclusions of the thesis [27] that the most suitable type of filter in terms of meeting the criteria and usability is the Butterworth IIR filter.

The Butterworth filter is characterized by the maximum flatness of the passband and, at the same time, rolling off toward zero in the stopband. It is also referred to as a maximally flat magnitude filter. This feature guarantees the minimum possible distortion of the useful signal and, at the same time, avoids the amplification of higher harmonic components of deterministic interference. For these reasons, we do not consider other types of IIR filters, such as the Chebyshev filter, the Inverse Chebyshev filter, or the Cauer filter, which are characterized by a certain ripple in the pass or stopband.

Filter design specifications were obtained using the kurtogram method. The outputs of this method provide the information about the center frequency and bandwidth that we want to maintain. The Butterworth filter was implemented through the following syntax.

```
[b,a] = butter(order,[fc-bw/2 fc+bw/2]/(fs/2));
    y = filter(b,a,x);
```

- `order` is the filter order ($order = 6$),
- `b,a` are the transfer function coefficients,
- `x` is the input signal,
- `y` is the output signal (filtered signal).

A transfer function for a linear, time-invariant, causal digital filter can be expressed as a transfer function in the Z-domain [28]:

$$H(z) = \frac{B(z)}{A(z)} = \frac{b_0 + b_1 z^{-1} b_2 z^{-2} + \cdots + b_N z^{-N}}{1 + a_1 z^{-1} + a_2 z^{-2} + \cdots + a_M z^{-M}} \tag{4.3}$$

where the order of the filter is the greater of N or M, a and b are the filter transfer function coefficients.

The selected filter order was set to six. This filter order is a compromise between computational complexity and filter selectivity. For a larger filter order, the transition bandwidth decreases, and thus the selectivity of the filter increases (see figure 12). This also guarantees the filtering of higher harmonic components of deterministic interference. The output parameters of the illustrated kurtogram lead to a high-pass filter. However, for example, for a stationary type of bearing fault signal, the kurtogram generates parameters that lead to a bandpass filter [5]. For this reason, the filtering algorithm is ready for this type of filter and thus meets the requirements for selectivity.

The transfer function of the designed filter using the parameters obtained from the Kurtogram method is displayed in the figure 12.

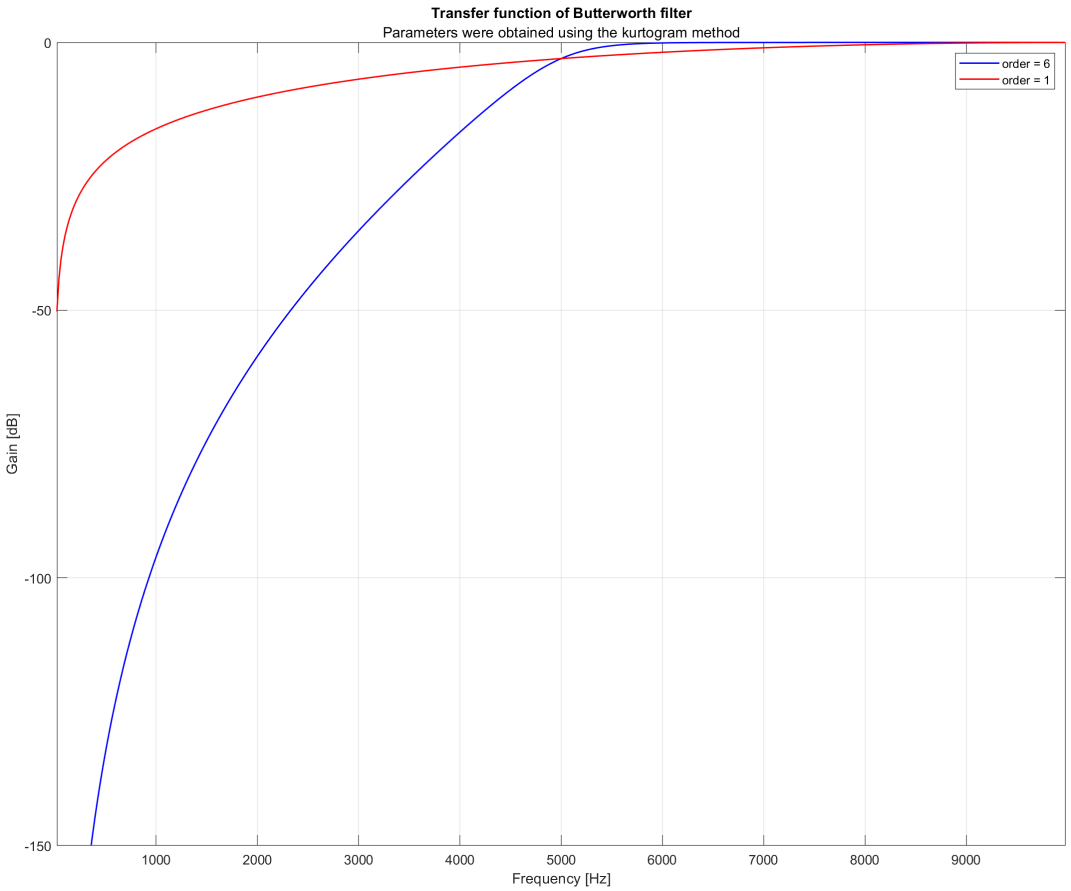

Figure 12: Illustration of the transfer function of the designed Butterworth filter with the parameters obtained using the kurtogram method. Blue = Butterworth filter with order equal to 6, red = Butterworth filter with order equal to 1.

A comparison of the raw signal with the deterministic components and the output of the designed filter withe the order equal to six can be seen in the figure 13. We can observe successful filtering of low-frequency interference of deterministic components.

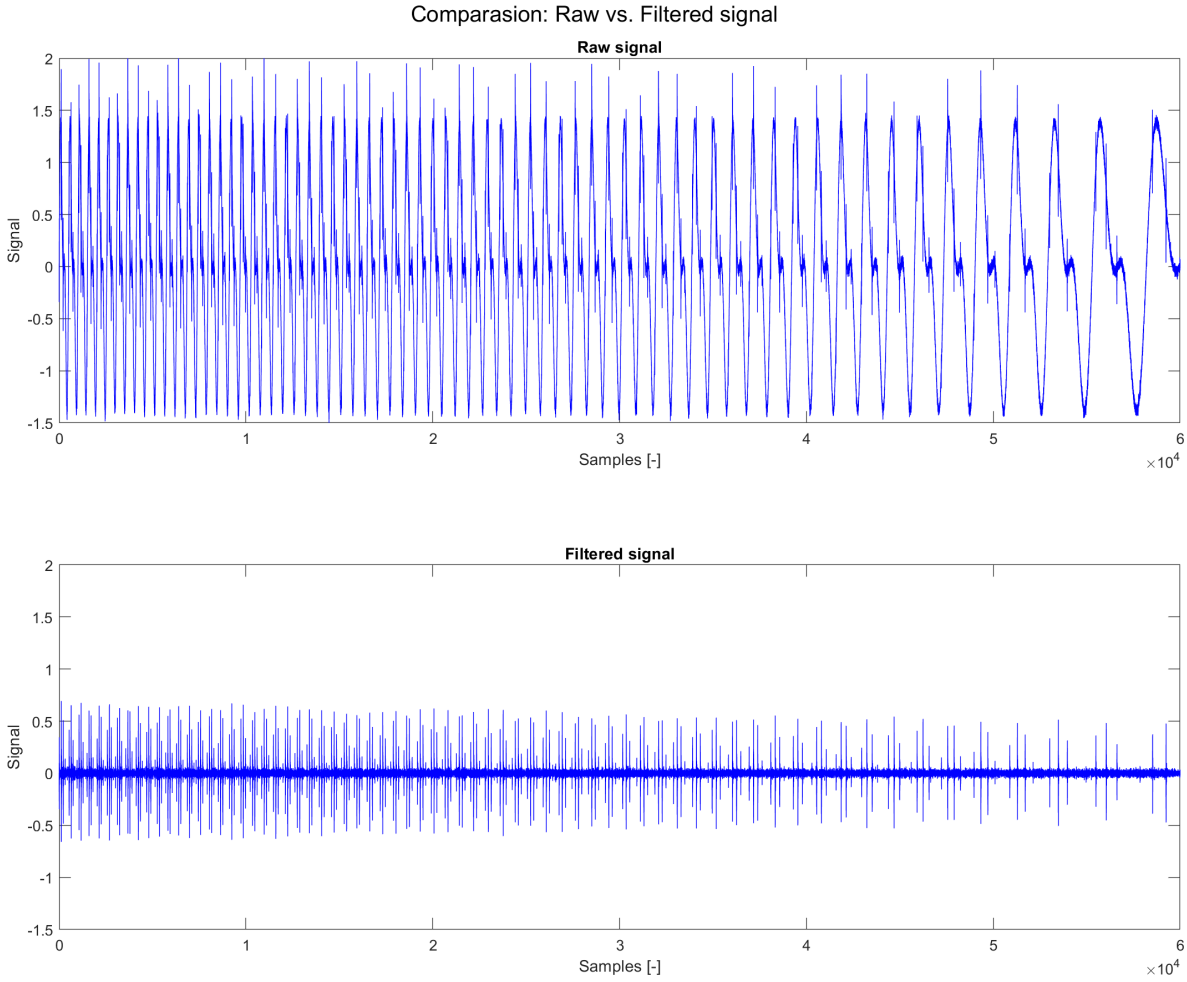

Figure 13: Figure showing a comparison of the time course of the raw signal (top) and the filtered signal (bottom).

4.3.2 Signal segmentation

The output signal of the filter was then segmented into windows with a length of 2000 samples. This value was determined from the analysis of the most dynamic signal from the created database using the kurtogram method. For values less than 2000 samples, the kurtogram method did not provide consistently accurate values. The consequence of such segmentation was a reduction in the dynamics of non-stationary processes within a single window. The

advantage of this approach was the possibility of checking the results for individual windows and thus correctly optimizing the entire analysis process.

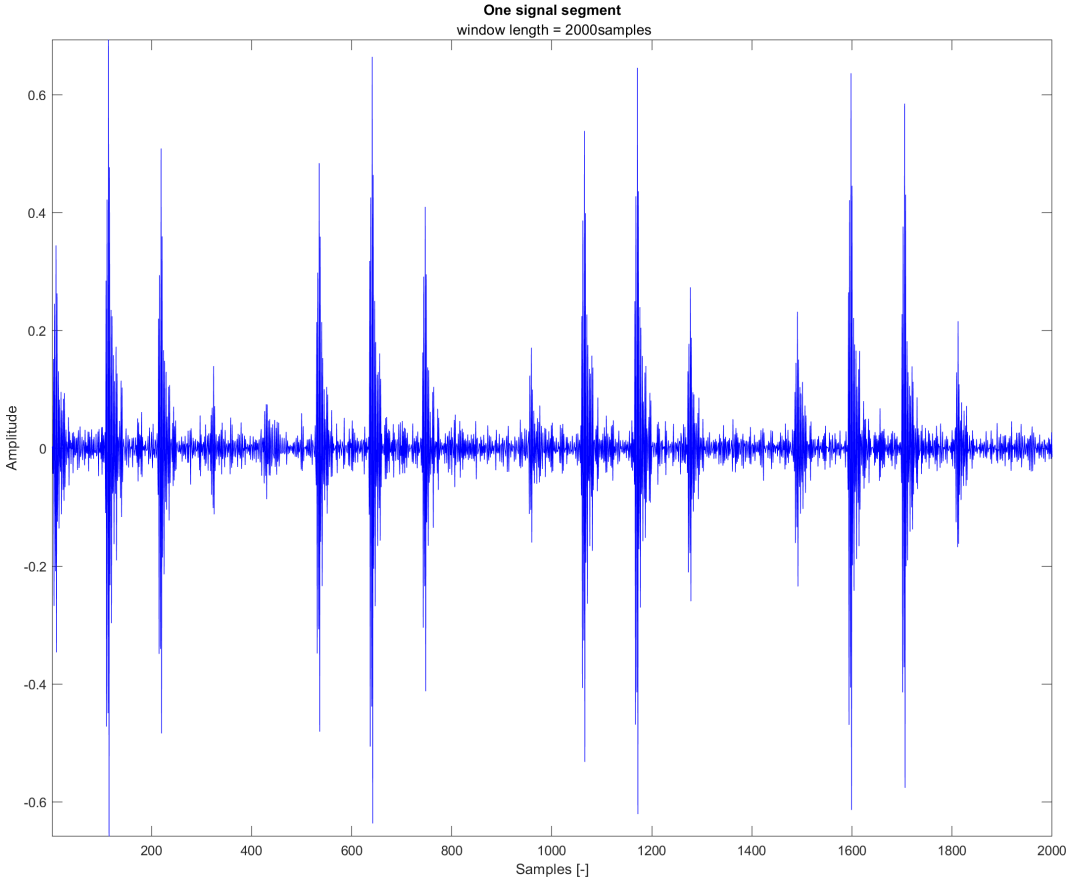

Figure 14: Display of the signal course within one segment with a length of 2000 samples.

4.4 Power Spectral Density

The power spectrum of a signal describes the distribution of power into frequency components composing that signal [29]. The graphical representation of this method is called the periodogram. The calculation of the power spectral density was performed in this work using the Welch's method.

Welch's method computes a PSD for each segment and then averages these estimates to produce the estimate of the power spectral density. Because the process supposed to be wide-sense stationary and Welch's method uses PSD estimates of different segments of the time series, the smoothed periodograms represent approximately uncorrelated estimates of the true PSD and averaging reduces the variability.

The reason why the power spectral density calculation was used is that this step was used to obtain information about the frequency band, where the information about the useful signal is contained within the given window.

The cut-off frequencies of such a frequency band of interest were determined by the intersection of the set threshold and the power spectral density. The threshold was set at 3·mean of power spectral density. This value is the result of compromising the noise resistance of the analysis and determining the useful frequency band where the vibration pulses are contained (see Figure 15).

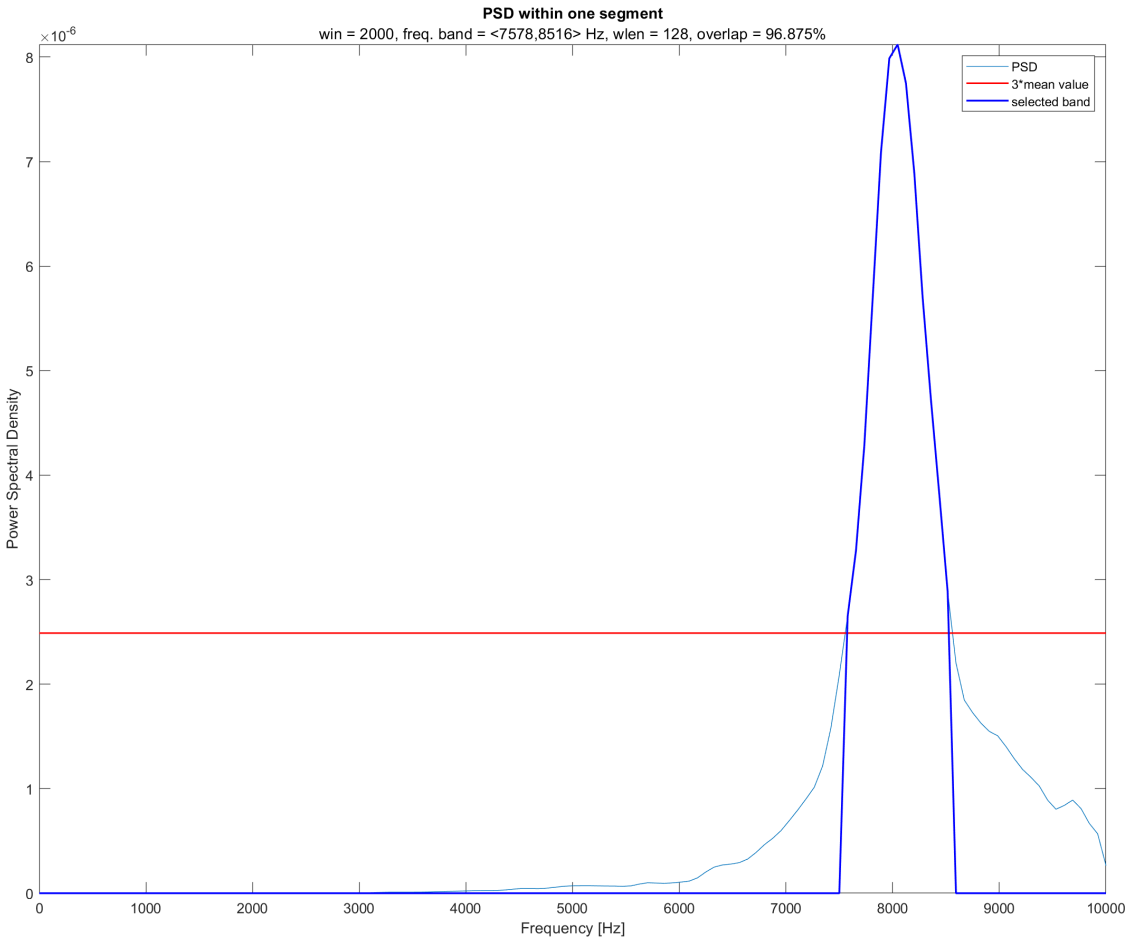

Figure 15: Figure showing the Welch's power spectral density of one segment (light blue), the threshold value (red) and the selected frequency band (blue). The specified band for this segment ranges from 7578 Hz to 8516 Hz.

4.5 Short-time Fourier transform

The Short-time Fourier transform (STFT), is a modification of Fourier transform used to determine the spectral content of local sections of a signal as it changes over time [23]. The two-dimensional representation of squared magnitude of the STFT is called the **spectrogram**, which is a helpful visualization of the temporal evolution of the spectral content of the analyzed signal.

The reason why this method is used is that the spectral values from obtained frequency band of interest (see section 4.4) are projected from the spectrogram to the time axis by summing the frequencies in the given band at a given time within one signal segment (see section 4.3.2). After performing this operation, we get a kind of envelope of vibration pulses.

The STFT of a signal is calculated by sliding an analysis window of length M over the signal and calculating the discrete Fourier transform of the windowed data (see Figure 16). After analyzing the properties of different types of windows, the Hann window type was used in this work. L specifies the length of overlap in samples. The overlap-adding of the windowed segments compensates for the signal attenuation at the window edges. Thus, an undesirable phenomenon called spectrum leakage is treated. The DFT of each windowed segment is added to a matrix that contains the magnitude and phase for each point in time and frequency. The number of rows in the STFT matrix equals the number of DFT points, and the number of columns is given by

$$k = \left\lfloor \frac{N-L}{M-L} \right\rfloor \tag{4.4}$$

where N is the length of the input signal x in samples, M is the window length, L specifies the overlap-adding in samples.

The STFT matrix is defined as follows.

$$X(f) = [X_1(f)X_2(f)X_3(f)\cdots X_k(f)] \tag{4.5}$$

The m-th elemnt of the matrix $X(f)$ is equal to

$$X_m(f) = \sum_{n=-\infty}^{\infty} x(n)g(n-mR)e^{-j2\pi fn} \tag{4.6}$$

where $X_m(f)$ is the DFT of windowed data centered about time mR, $g(n)$ is the window function of length M, R is the hop size between successive DFTs. The hop size is defined as $R = M - L$ [23].

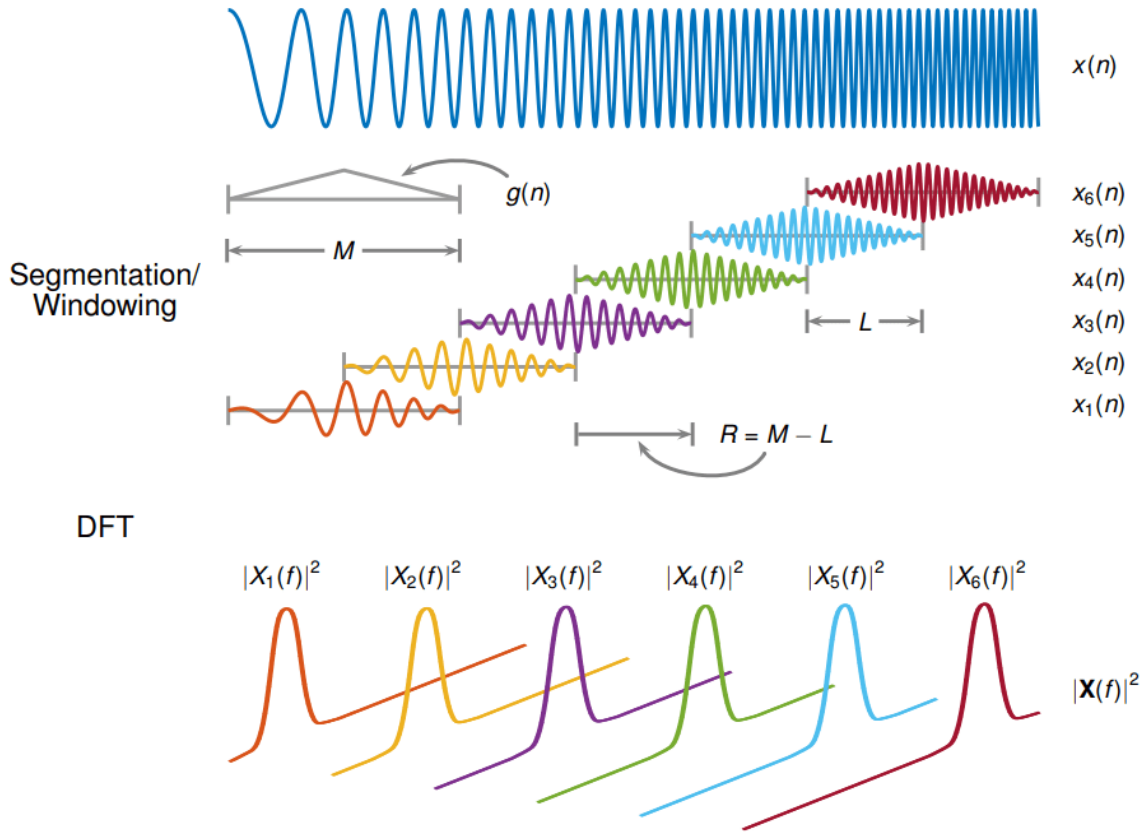

Figure 16: Graphical representation of the described STFT algorithm leading to a two-dimensional graphical representation of the squared magnitude of the STFT called the spectrogram [4]. $x(n)$ is the input signal, $g(n)$ is the window function of length M, L defines the overlap in samples, the hop size between successive DFTs is defined as $R = M - L$.

4.5.1 Window length analysis

As mentioned in chapter 4.2, the window length is one of the critical parameters affecting the resulting STFT value. Therefore, the following study was performed comparing the effect of window length on the accuracy of the calculation of the value of the period of vibration pulses. Due to this analysis, the optimal window length will be obtained.

The reason why the length of the window is so crucial is that the length of the window in STFT calculation relates to how the signal is represented. It determines whether there is good frequency resolution (frequency components close together can be separated) or good time resolution (the time at which frequencies change). A wide window gives better frequency resolution but poor time resolution. A narrower window gives good time resolution but poor frequency resolution. This phenomenon can be observed in Figure 17.

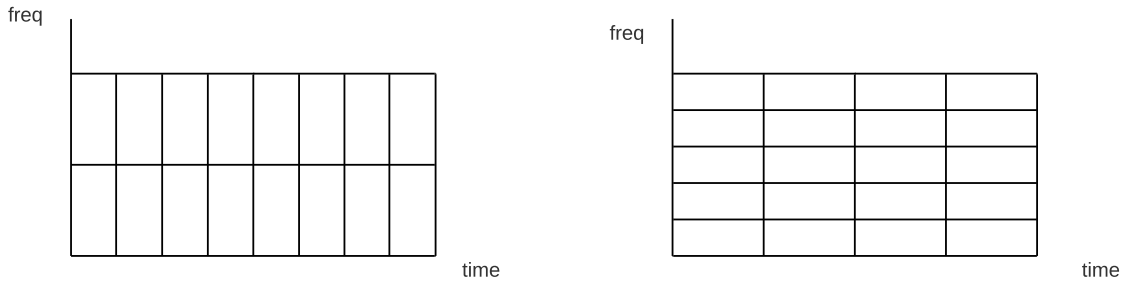

Figure 17: Illustration of the impact of window length on STFT time-frequency resolution. A wide window gives better frequency resolution but poor time resolution (right). A narrower window gives good time resolution but poor frequency resolution (left).

For the following analysis examining the optimal length of the STFT window, the most dynamic signal from the created database with the following properties was selected:

- Fault type = Inner race fault,
- $f_{start} = 40$Hz,
- $f_{stop} = 5$Hz,
- $T = 3$s,
- $f_s = 20000$Hz,
- $SNR = 20, 30, 60$dB.

where f_{start} is the initial value of the shaft frequency speed f_r, f_{stop} is the frequency of f_r at the time of the signal duration T, SNR is the signal-to-noise ratio.

The comparison parameter was used to determine the correctness of determining the value of the period of vibrational pulses. Thus, the difference between the values determined by the proposed analysis and the values theoretically calculated (see equation (2.2)) using the Mean squared error (MSE) metric was determined. Overlap parameter was set to 75% of window length.

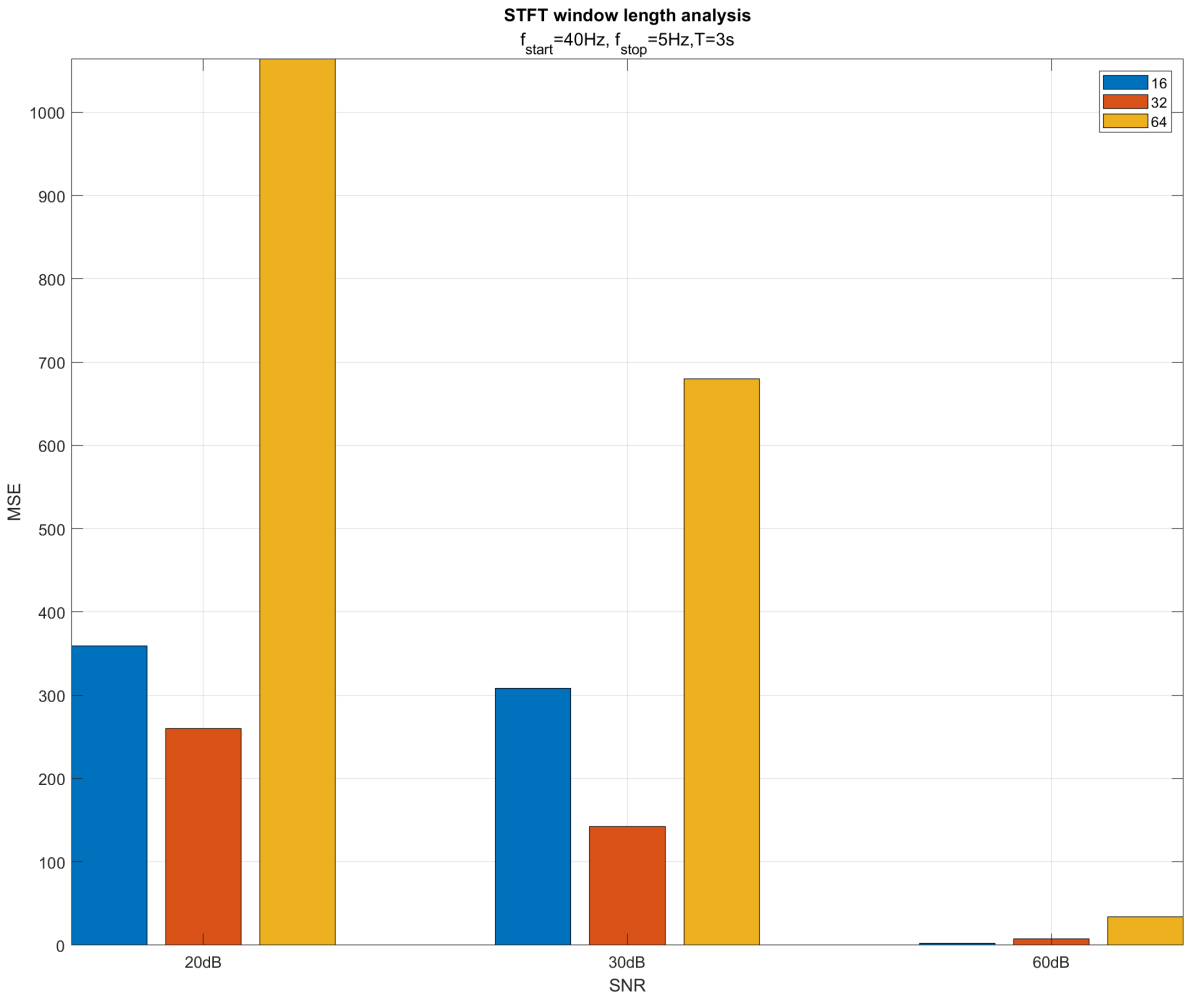

Figure 18: Displayed analysis results to determine the optimal length of the STFT window. For individual SNR values, the MSE value for a given STFT window length was plotted (the smaller the MSE value, the better). blue = 16 samples length, orange = 32 samples length, ocher = 64 samples length.

Window lengths of 8, 16, 32, 64 and 128 samples were considered for the analysis. But after the analysis, the 8 and 128 sample windows were discarded due to too high MSE values, which resulted in poorer readability of the graphical output of the analysis. The optimal length of the STFT window of 32 samples is based on the results of the performed analysis (see Figure 18). It would be possible to consider a window length of 16 samples, but due to the greater noise robustness of the results with a window length of 32 samples, the length of 32 samples was chosen as the optimal length of the STFT window for the purposes of the proposed signal analysis.

The figure 19 shows the impact of time-frequency resolution depending on the selected

length of the STFT window. The selected window length is always a compromise between a more detailed frequency or more detailed time resolution.

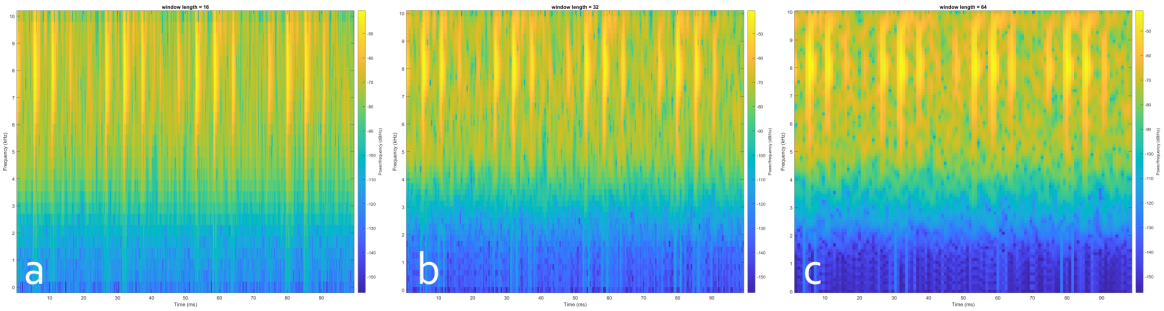

Figure 19: Displayed spectrograms within one signal segment for window lengths of: a) 16, b) 32, c) 64 samples. The warmer the color, the more energy there is at a given frequency. X-axis = time [ms], Y-axis = frequency [kHz].

4.5.2 Overlap length analysis

Another critical parameter of the Short-time Fourier transform is the length of overlap of individual STFT windows (see Figure 16). The analysis was performed on a similar principle as in the analysis of the influence of the length of the STFT window on the analysis result. The difference in this analysis was that the optimal value of the STFT window length is known from the previous study, and it is equal to 32 samples. The parameter that was examined was the length of the overlap of the STFT window. The values of such overlaps were chosen to be 16, 24, 28, and 31 samples.

The results of the performed analysis (see Figure 20) indicate the fact that an overlap of 31 samples (97% of the window length) is the best value for the purposes of plausibility of the results of the performed signal analysis. Due to the lower value of the MSE metric, the results determined from the analysis are more similar to the theoretically calculated results than the results with a higher MSE value.

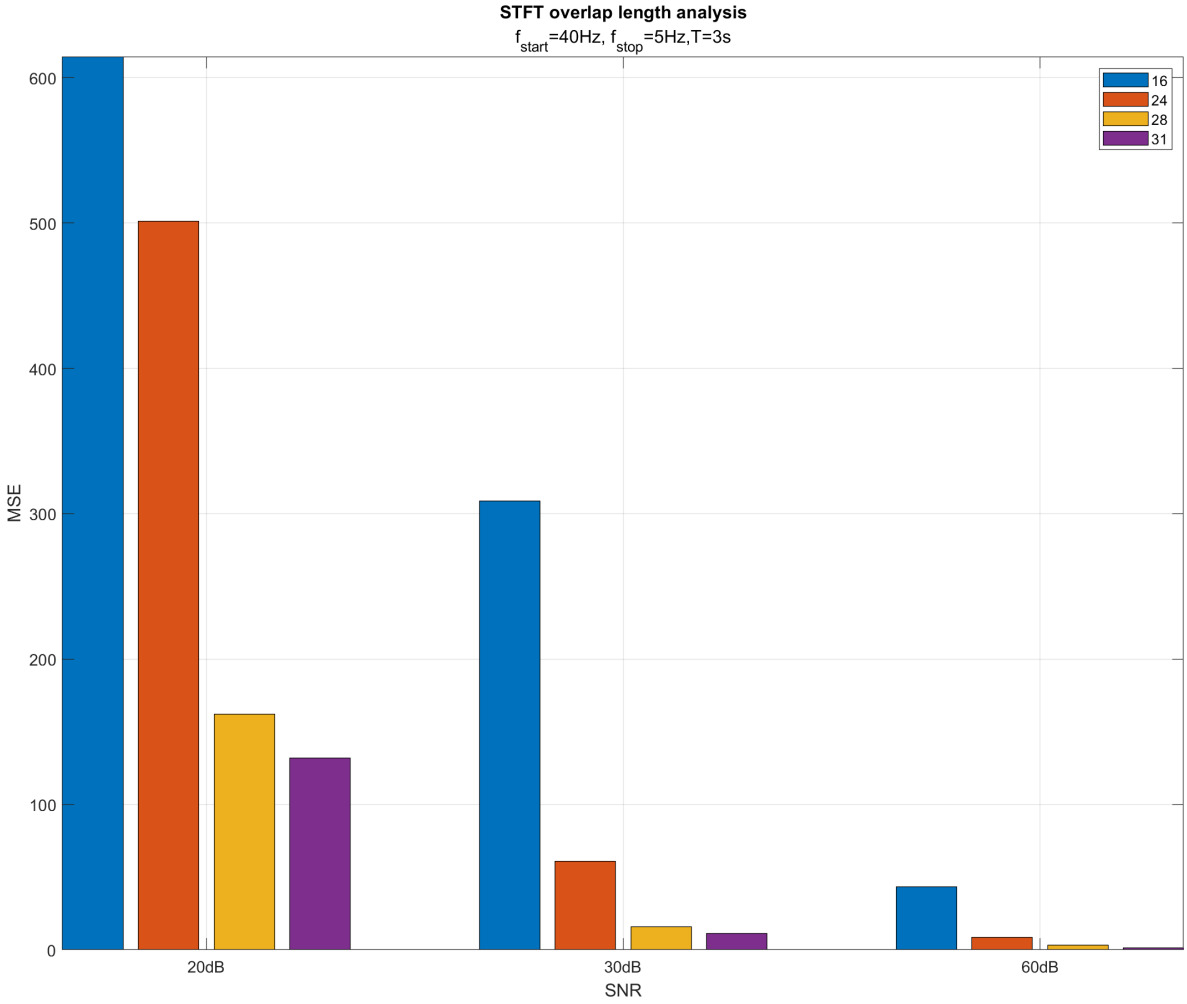

Figure 20: Displayed analysis results to determine the optimal length of the STFT window overlap. For individual SNR values, the MSE value for a given overlap length was plotted (the smaller the MSE value, the better). blue = 16 samples length, orange = 24 samples length, ocher = 28 samples length, purple = 31 samples length.

4.6 Fourier Synchrosqueezed transform

The time-frequency resolution (see section 4.5.1) limits the transformation of the Short-time Fourier transform mentioned in the previous chapter. One of the approaches that try to solve this problem is the Fourier Synchrosqueezed transform [24].

The synchrosqueezing is a post-processing method that circumvents the uncertainty relation inherent to the linear transform STFT, by reassigning the coefficients in scale or frequency [30].

The aim of the FSST is threefold:

- to sharpen a time-scale representation,
- to sharpen at frequency domain,
- remaining invertible.

Generated bearing fault signals can be expressed as a superposition of amplitude-modulated and frequency-modulated modes. For time-frequency analysis, it is convenient to express such signals as sums of analytic signals through

$$f(t) = \sum_{k=1}^{K} A_k(t) e^{j2\pi\phi_k(t)} \tag{4.7}$$

where A_k are the instantaneous amplitudes and ϕ_k are the instantaneous phases.

The Fourier synchrosqueezed transform (FSST) is based on the short-time Fourier transform of a fucntion f (see section 4.5) which is defined as follows

$$V_g f(t,\eta) = \int_{-\infty}^{\infty} f(x) g(x-t) e^{-j2\pi\eta(x-t)}\, dx \tag{4.8}$$

where g represents the spectral window.

The STFT coefficients $V_g f(t,\eta)$ are subsequently squeezed so that they concentrate around curves of instantaneous frequency $\Omega_g f(t,\eta)$ in the time-frequency plane (equation (4.10)).

$$\Omega_g f(t,\eta) = \frac{1}{j2\pi} \frac{\frac{\partial}{\partial t} V_g f(t,\eta)}{V_g f(t,\eta)} \tag{4.9}$$

This type of evaluation decreases the influence of the window [30].

The resulting **synchrosqueezed transform** is defined as follows.

$$T_g f(t,\omega) = \int_{-\infty}^{\infty} V_g f(t,\eta) \delta(\omega - \Omega_g f(t,\eta))\, d\eta \tag{4.10}$$

The Fourier Synchrosqueezed transform was performed in the Matlab® environment using the `fsst` function, which has the following syntax.

```
[s,f,t] = fsst(x,fs,window(length);
```

- `x` is the input signal,
- `fs` is the sampling frequency ($fs = 20000$ Hz),
- `window` defines the window type and length of the window in samples ($window = hann(64)$).

The selected window length of 64 samples was the value that gave the best signal analysis results. This value was determined from the same method of analysis to determine the optimal window length as in the previous chapter Short-time Fourier transform (see chapter 4.5.1). It is worth mentioning that the window overlay cannot be defined for the fsst function. This is because this function is defined for a fixed parameter value that is equal to $overlap = windowLength - 1$ in samples.

The output of the fsst function is the so-called fsstgram. It is a modified method of the spectrogram. A comparison of the graphic outputs of Short-time Fourier transform (spectrogram) and Fourier Synchrosqueezed transform (fsstgram) is shown in the following figure 21. It can be observed that the visible sharpening of the fsstgram in the frequency domain is present.

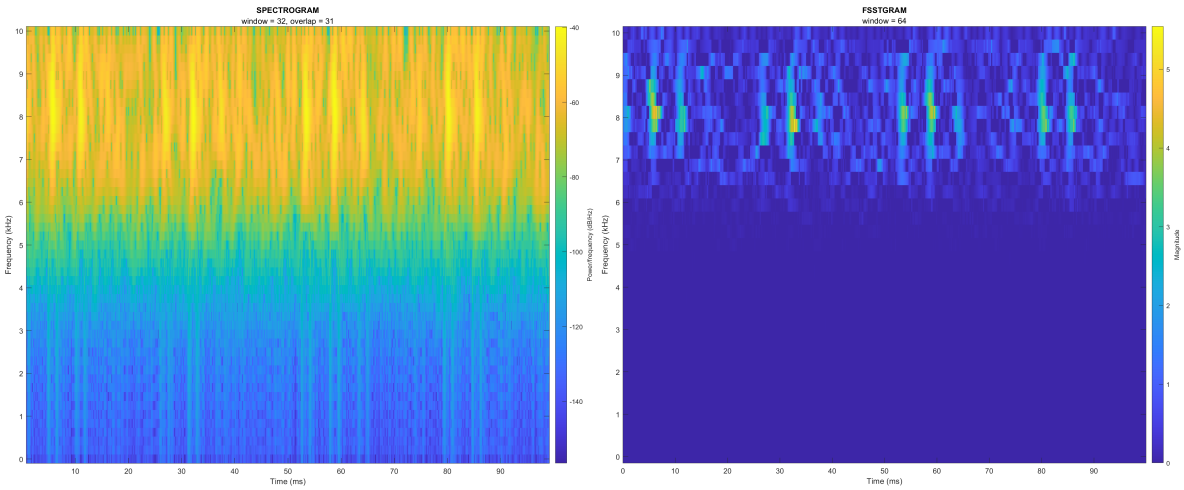

Figure 21: A comparison between spectrogram (left) and fsstgram (right) within one segment. X-axis = time [ms], Y-axis = frequency [kHz].

4.7 Localization of pulses using the spectral region

Due to time-frequency analysis using STFT or FSST, we can project the spectral components to the time axis. This gives us some form of the pulse envelope (see figure 22). Thanks to the knowledge of the frequency band of interest from the chapter 4.4, we will limit the projection of spectral components to this band thus this can be understood as a filtration in frequency domain. The projection of spectral components to the time axis is given by the following equation.

$$s_{pulse}(t) = \sum_{i=f_{low}}^{f_{high}} s(t, f_i) \qquad t\epsilon\langle 0, T\rangle \quad (4.11)$$

where s is the output of spectrogram or fsst function, t is the time duration of the analysed segment, f_{low} and f_{high} are the frequencies defining the frequency band of interest which were obtained from section 4.4.

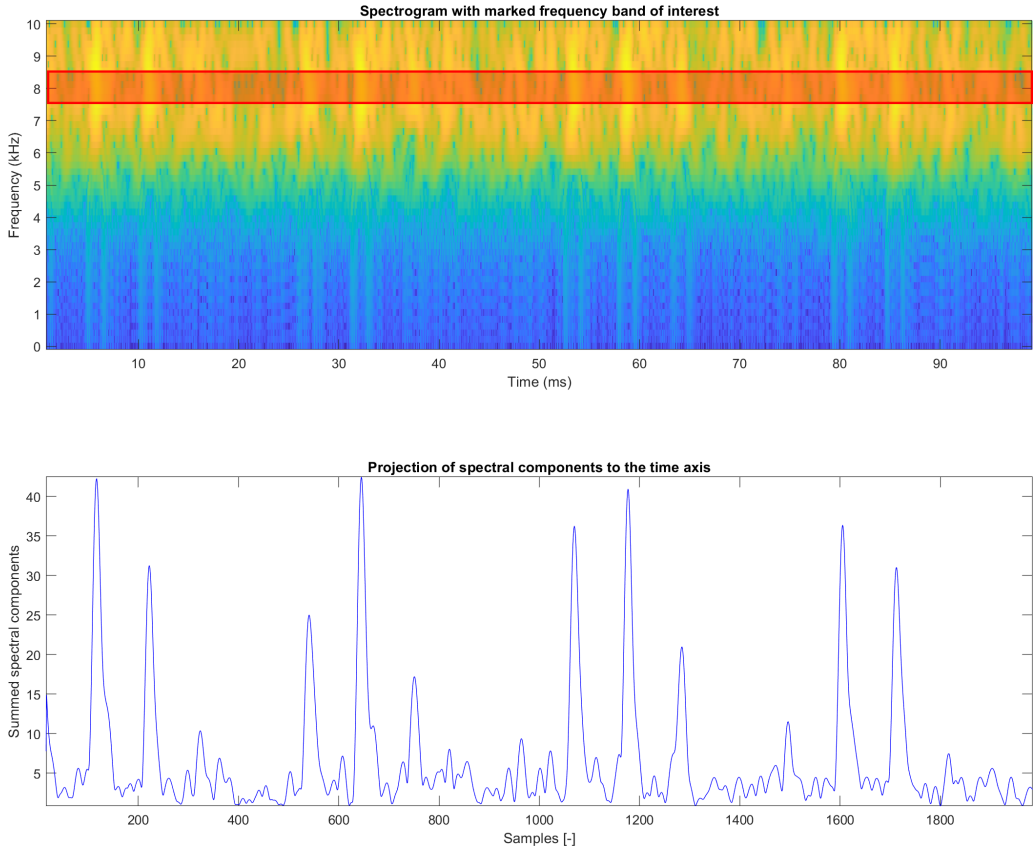

Figure 22: Spectrogram of one segment with marked frequency band of interest (top). Projected spectral components to the timeline using the displayed spectrogram (bottom).

Using the operation of integrating the resulting signal obtained by projecting the spectral components to the time axis, we obtain one value corresponding to the surface of the resulting envelope of each pulse. This results in the ability to determine the position of the pulse over time unambiguously. It is important to mention that the integration operation takes place from a set threshold (see Figure 23). This threshold was set to a base value equal to $threshold = Kmean(s_{pulse})(t)$, where $K \epsilon \mathbb{R}$ is a factor by which we can influence the threshold value as needed depending on the degree of noise in the signal. The value of factor K was chosen experimentally.

The resulting integration values are stored in a row vector for the purpose of continuously storing these values for other signal segments.

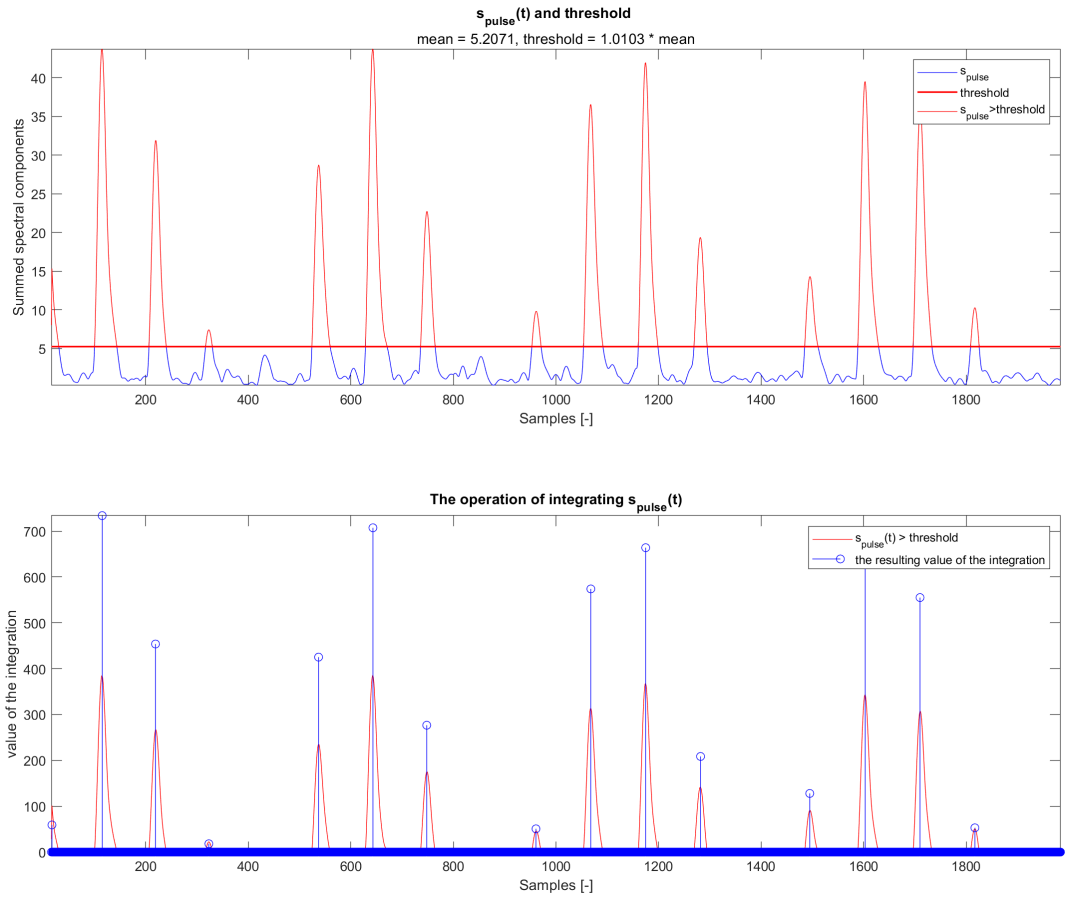

Figure 23: Display of the time course of projection of spectral components to the time axis with the marked threshold value for integration purposes (top). The resulting values of integration (bottom).

4.8 The fault frequency determination

After analyzing the last segment of the signal, it is possible to determine the distance between the individual pulses, which corresponds to the time evolution of the period corresponding to $\frac{1}{BPF}$. The term BPF is intentionally given here because the specific type of fault is not yet known, and therefore we cannot clearly determine whether it is an inner race fault or an outer race fault.

After determining the length of the fault period, it was necessary to correct the resulting data from incorrectly determined data. If the resulting period between two pulses was approximately twice as long as the length of the previous period, it means that one pulse was not detected. Therefore, the longer period was shortened to a value corresponding to the length of the previous period, and at the same time, a new value of the period of the same length as the previous period was added at position $n + 1$, where n corresponds to the position of the originally twice long period (see Figure 24). The resulting length of the vector containing all the period length values was increased by one value by this step.

On the other hand, if a value significantly lower (approximately three times lower) appeared in the resulting fault period vector than the previous value, this value was deleted, and the resulting vector was shortened by one sample by this operation.

At this point, it was possible to compare the correctness of determining the time evolution of the values of the fault frequency BPF corresponding to the value $\frac{1}{BPF_{period}}$ with the vector corresponding to the generated fault frequency of individual pulses of the given signal. Mean squared error (MSE) was determined as a metric to determine the similarity of the two signals (see Figure 24).

It can be seen from the figure 24 that the detection of the development of the BPF frequency is not error-free, but more or less tries to copy the course of the generated BPF values. The accuracy of the determination depends on the degree of noise in the signal. Thus, the smaller the SNR value, the less accurate the determination.

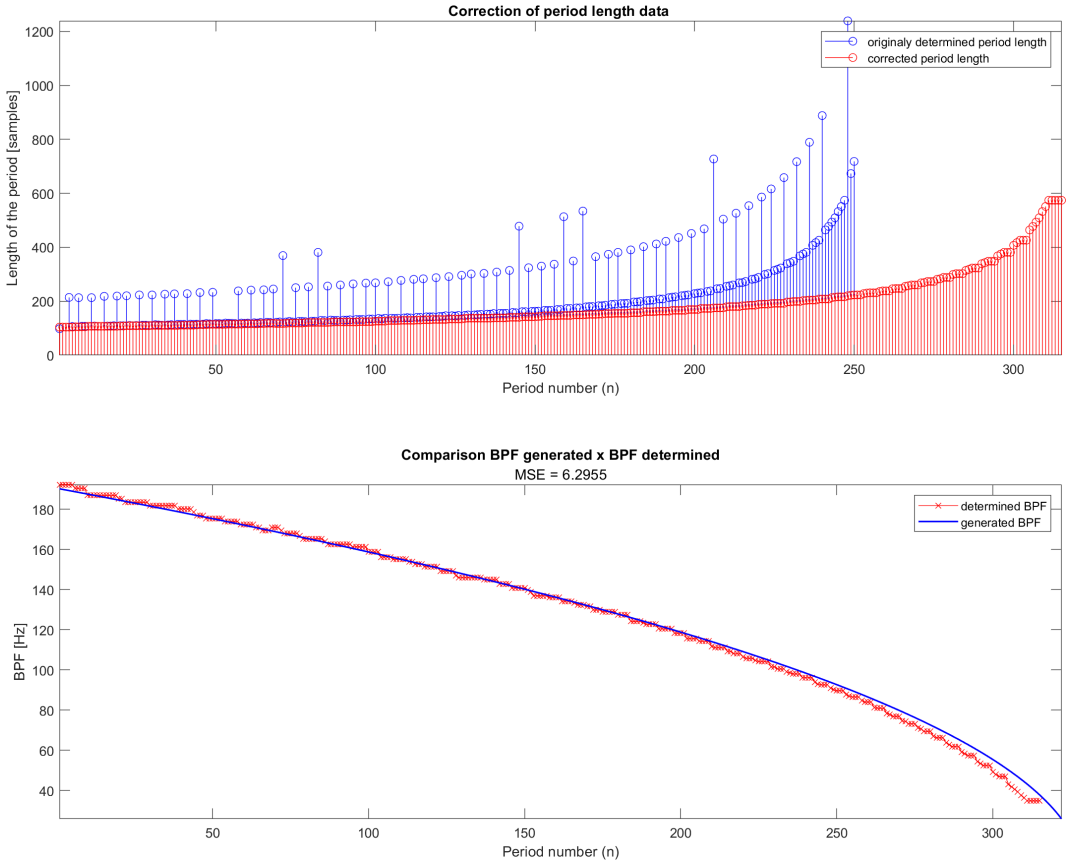

Figure 24: Figure showing the correction of the determined period lengths corresponding to $\frac{1}{BPF}$ (top) and a comparison of the time evolution of the BPF frequency (red) with the generated BPF values (blue) (bottom). The MSE value defines the similarity of the two vectors, and thus the lower the MSE value, the similar these vectors are.

4.9 Determination of the fault type and shaft rotation speed frequency

The advantage of the generated data is the fact that it was possible to store the development values of the theoretically calculated BPFO and BPFI values (see equations (2.1) - (2.2)) depending on the change of the shaft rotation speed frequency.

Therefore, determining the type of defect is relatively straightforward. Using the MSE metric, the theoretically calculated BPFI and BPFO values were compared with the determined values of the failure frequency of an unspecified BPF type (see chapter 4.8). The resulting type of fault was therefore determined using the smaller of the two MSE values.

Due to the knowledge of the fault type, specific bearing type, and the time evolution of the fault frequency (BPFI or BPFO), we can calculate the course of the time evolution of the shaft speed frequency f_r by modifying the equations (2.1) - (2.2) as follows.

- f_r determined using BPFO frequency = **Outer race fault**

$$f_r = \frac{2BPFO}{(1 - \frac{d}{D})n} \quad \text{[Hz]} \quad (4.12)$$

- f_r determined using BPFI frequency = **Inner race fault**

$$f_r = \frac{2BPFI}{(1 + \frac{d}{D})n} \quad \text{[Hz]} \quad (4.13)$$

where f_r is the shaft speed frequency in Hz, $BPFO$ or $BPFI$ are the determined fault frequencies of specified fault type in Hz, d is the rolling element diameter, D is the pitch diameter and n is the number of rolling elements.

The resulting time course of the determined shaft speed frequency and the generated shaft speed frequency can be seen in the figure 25.

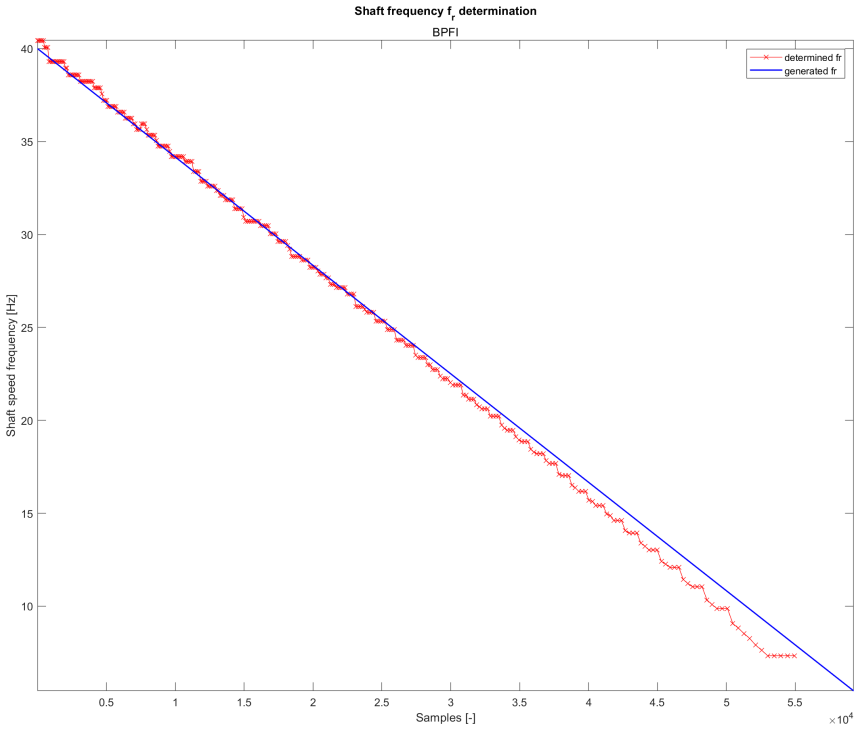

Figure 25: The determined time evolution of the shaft speed frequency using BPFI (red) compared to the time evolution of the generated shaft speed frequency (blue).

The Figure 25 was generated for method control purposes. It can be seen that the results of determining the shaft speed frequency value over time correspond to some extent to the generated values. A certain deviation occurs at lower frequencies, when there is a smaller number of pulses within a segment with a length of 2000 samples and thanks to that the method is less accurate.

In order to demonstrate a better result of determining the time evolution of the BPF fault frequency, the following figure 26 was added to this work. The type of bearing fault analyzed here is the outer race fault, which is a better detectable fault using the proposed detection method, as the next chapter shows (see chapter 5). Compared to the figure 24, it is both visually and numerically (MSE value) justified that determining the course of the BPF error frequency is better for the case of the figure because the determined course more closely copies the course of the generated value.

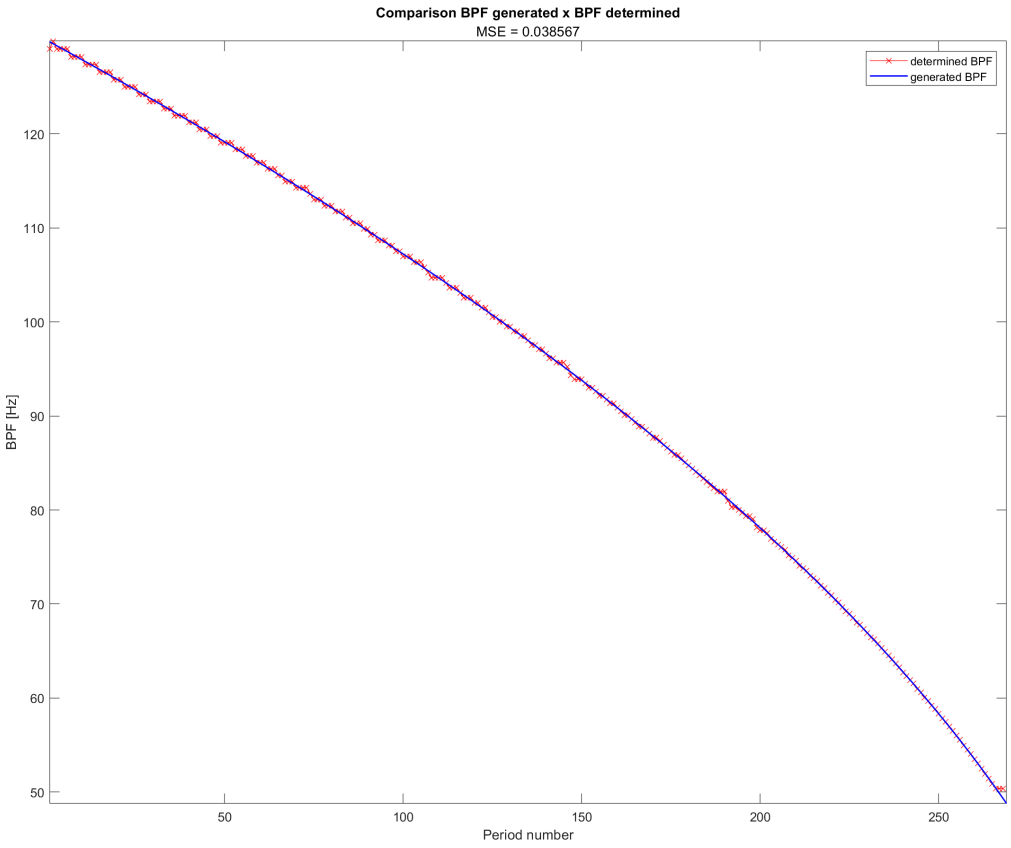

Figure 26: Outer race fault. A comparison of the time evolution of the BPF frequency (red) with thegenerated BPF values (blue). The MSE value defines the similarity of the twovectors, and thus the lower the MSE value, the similar these vectors are.

Chapter 5

Signal analysis of the created non-stationary bearing fault database

This chapter briefly discusses the application of the developed method of signal analysis for bearing fault detection under non-stationary conditions. Generated signals from the created non-stationary bearing fault database (see 3.5) were used as input data to the signal analysis. Primarily, this chapter is intended to compare the results of the two methods used, which are spectrogram and fsstgram (see Figures 27 - 32).

The signal analysis procedure was divided into four categories according to the type of fault and the type of transformation that was used.

Division by the fault type:

- Outer race fault,
- Inner race fault,

Division by the transformation type:

- Short-time fourier transform (spectrogram),
- Fourier Synchrosqueezed transform (fsstgram),

The signals from created database were analyzed according to the algorithm described in the chapter 4. The result of the analysis, which is a determination of the time evolution of the fault frequency (BPF), was compared with the expected result of the time evolution of the BPF from the signal generator. The Mean squared error metric was used as a metric to compare the similarity of these signals (see chapter 4.8).

A complete description of signals from the non-stationary signal database can be found in the Attachments section in the tables 6.1 - 6.2. Likewise, the results of the analysis of this database can be found in the Attachments section in the form of bar graphs 27 - 32.

From the results of the analysis we can determine two basic conclusions, which must be understood as conclusions related only to the form used of all created methods and algorithms, but not as generally valid conclusions.

First, the fsstgram method is less suitable for bearing fault detection than the spectrogram method due to its lower robustness to noise interference. From the resulting graphical outputs (see Figures 27 - 32) it can be seen that the Mean squared error (MSE) value increases very steeply with decreasing SNR level. However, at high SNR values, both methods, spectrogram and fsstgram, give similar results, especially for the bearing fault detection in case of outer race fault.

Second, detecting the inner race faults is more difficult than detecting outer race faults. This is caused primarily by the presence of amplitude modulation in the signal in which the inner race fault type occurs. Pulses that have a very reduced amplitude due to amplitude modulation are easily lost in the noise-affected area. This makes it impossible to successfully detect all pulses at lower SNR values. In contrast, the detection of an outer race fault is relatively successful for both types of methods used. However, even here the rule applies that the fsstgram method is less robust to additive noise at lower SNR values than the spectrogram method.

Chapter 6

Conclusion

All set points in the thesis assignment were met.

In the chapter 2, the reader was introduced to the issue of the origin and detection of bearing faults. Individual types of bearings and individual types of bearing faults were mentioned. The principle of detection of these faults was described, and the illustrative course of signals of individual types of bearing faults was shown. At the end of the chapter 2, the procedure for determining the frequency of the fault depending on the shaft speed frequency is mentioned.

In the following chapter 3, a generator of non-stationary bearing fault signals was created. Using the analysis of available databases, the necessary parameters to create relevant signals were determined. In particular, it is a time constant τ, which was set to the value $\tau = 0.0005$ s. Another important parameter determined is the resonant frequency of the system f_c, which was set to the value $f_c = 8000$ Hz. These values were used to generate Inner race fault and Outer race fault signals. Nonstationarity was modeled using a time change of shaft speed frequency. A bearing deceleration scenario was used. The Non-stationary Bearing Fault Signal Database was created using a bearing fault signal generator. This database was created and described for experimental purposes.

In Chapter 4, an algorithm of the developed method was created in order to detect bearing faults under non-stationary conditions. This algorithm is described using a block diagram (see Figure 10). The individual methods that were used are described in more detail, and the selected parameters of these methods are mentioned. The method known as the Kurtogram was used to determine the optimal parameters of the analyzing methods. These methods are namely spectrogram and fsstgram. The selection of other input parameters of these methods is discussed in more detail and, in most cases, is based on the analysis of different parameter values in order to determine the optimal values. Using the proposed method of fault detection, the characteristic vibration pulses of these faults were detected. Subsequently, the time

evolution of the BPF fault frequency was determined, and the type of fault was determined. Thanks to the knowledge of the mathematical relationships between the shaft frequency speed and the fault frequency of the given type, which were mentioned in Chapter 2, the time course of the shaft speed frequency was determined.

In the last chapter, an analysis was performed using the proposed method (see Chapter 4) in order to compare the spectrogram and fsstgram methods used. Generated signals from The Non-stationary Bearing Fault Signal Database were used as input data. All analysis results can be found in the Attachments section in the form of bar graphs (see Figure 27 - 32). Due to the good readability of the graphs, it is necessary to pay attention to the scale of the plotted graphs. Two conclusions can be drawn from the results, which, however, should not be perceived as a general truth. First, less robustness of the fsstgram method to additive noise can be observed at lower SNR values. Second, detecting an inner race fault is more complex than detecting an outer race fault. This is caused by the presence of amplitude modulation in the signal containing this type of fault. As a result, pulses with small amplitude are lost in the noise-affected area and therefore cannot be detected.

The author sees an option for future expansion or improvement of this work, mainly in the improvement of the signal analysis method for the purpose of detecting bearing failures under non-stationary conditions. Better results would be achieved by improving the functionality of the Kurtogram method even at lower SNR values. Furthermore, the author sees the possibility of improvement in determining the integration threshold in an automatic way. This would lead to complete automation of the algorithm.

Bibliography

[1] University of Cambridge, "Mechanical bearings." [Online]. Available: https://www.phase-trans.msm.cam.ac.uk/2010/types/index.html

[2] S. Kim, D. An, and J.-H. Choi, "Diagnostics 101: A tutorial for fault diagnostics of rolling element bearing using envelope analysis in matlab," *Applied Sciences*, vol. 10, no. 20, 2020. [Online]. Available: https://www.mdpi.com/2076-3417/10/20/7302

[3] R. B. Randall and J. Antoni, "Rolling element bearing diagnostics—a tutorial," *Mechanical Systems and Signal Processing*, vol. 25, no. 2, pp. 485–520, 2011. [Online]. Available: https://www.sciencedirect.com/science/article/pii/S0888327010002530

[4] Mathworks. Short-time fourier transform. [Online]. Available: https://www.mathworks.com/help/signal/ref/stft.html

[5] O. Lahoda, "Detekce poruch ložisek," Master's thesis, České vysoké učení technické v Praze, 2021.

[6] Merriam-Webster.com Dictionary, "bearing." [Online]. Available: https://www.merriam-webster.com/dictionary/bearing

[7] American Bearing Manufactures Association, "Bearing timeline." [Online]. Available: https://www.americanbearings.org/page/bearing_timeline

[8] M. Kičák, "Návrh databáze pro měření stavu ložisek zabíhacích válců," Master's thesis, České vysoké učení v Praze, 2018.

[9] S. Alegranzi, J. Fagundes Gonçalves, and H. Gomes, in *Ball Bearing Vibration Monitoring for Fault Detection by the Envelope Technique*, 05 2014, pp. 4113–4125.

[10] T. A. Harris, *Rolling Bearing Analysis*. Wiley, 2001.

[11] B. T. Kuhnell, "Wear in rolling element bearings and gears - how age and contamination affect them," *Machinery Lubrication*, 2004. [Online]. Available: https://www.machinerylubrication.com/Read/664/wear-bearings-gears

[12] P. Vara prasad and V. Kumar, "Detection of bearing fault using vibration analysis and controlling the vibrations," *International Journal of Engineering Sciences and Research Technology*, vol. 4, pp. 539–550, 10 2015.

[13] N. Sawalhi, "Rolling element bearings localized fault diagnosis using signal differencing and median filtration," *Journal of Vibroengineering*, vol. 20, no. 3, pp. 1322–1339, may 2018. [Online]. Available: https://doi.org/10.21595%2Fjve.2017.18254

[14] M. Kunli and W. Yunxin, "Fault diagnosis of rolling element bearing based on vibration frequency analysis," in *2011 Third International Conference on Measuring Technology and Mechatronics Automation*, vol. 2, 2011, pp. 198–201.

[15] G. F. Franklin, D. J. Powell, and A. Emami-Naeini, *Feedback control of dynamic systems*. Prentice Hall PTR, 2001.

[16] H. Huang and N. Baddour, "Bearing vibration data collected under time-varying rotational speed conditions," *Data in Brief*, vol. 21, pp. 1745–1749, 2018. [Online]. Available: https://www.sciencedirect.com/science/article/pii/S2352340918314124

[17] E. Bechhoefer. Condition based maintenance fault database for testing diagnostics and prognostic algorithms. [Online]. Available: https://www.mfpt.org/fault-data-sets/

[18] J. Shi, M. Liang, and Y. Guan, "Bearing fault diagnosis under variable rotational speed via the joint application of windowed fractal dimension transform and generalized demodulation: A method free from prefiltering and resampling," *Mechanical Systems and Signal Processing*, vol. 68-69, pp. 15–33, 2016. [Online]. Available: https://www.sciencedirect.com/science/article/pii/S0888327015003817

[19] E. W. Weisstein. Sweep signal. [Online]. Available: https://mathworld.wolfram.com/SweepSignal.html

[20] H. Roder, "Amplitude, phase, and frequency modulation," *Proceedings of the Institute of Radio Engineers*, vol. 19, no. 12, pp. 2145–2176, 1931.

[21] D. HO and R. RANDALL, "Optimisation of bearing diagnostic techniques using simulated and actual bearing fault signals," *Mechanical Systems and Signal Processing*, vol. 14, no. 5, pp. 763–788, 2000. [Online]. Available: https://www.sciencedirect.com/science/article/pii/S0888327000913049

[22] H. F. Grip, W. Johnson, C. Malpica, D. P. Scharf, M. Mandić, L. Young, B. Allan, B. Mettler, and M. San Martin, "Flight dynamics of a mars helicopter," *NASA Ames Research Center*, 2017.

[23] A. V. Oppenheim, R. W. Schafer, and J. R. Buck, *Discrete-Time Signal Processing*, 2nd ed. Prentice-hall Englewood Cliffs, 1999.

[24] F. Auger, P. Flandrin, Y.-T. Lin, S. McLaughlin, S. Meignen, T. Oberlin, and H.-T. Wu, "Time-frequency reassignment and synchrosqueezing: An overview," *IEEE Signal Processing Magazine*, vol. 30, no. 6, pp. 32–41, 2013.

[25] J. Antoni, "Fast computation of the kurtogram for the detection of transient faults," *Mechanical Systems and Signal Processing*, vol. 21, no. 1, pp. 108–124, 2007. [Online]. Available: https://www.sciencedirect.com/science/article/pii/S0888327005002414

[26] O. M. Solomon Jr., *PSD Computation using Welch's method.* Sandia National Laboratories, 1991.

[27] A. Kubíček, "Odstraňování šumu z pohybových dat," Bachelor Thesis, 2018, České Vysoké Učení Technické v Praze.

[28] J. O. SMITH III. Introduction to digital filters. [Online]. Available: https://www.dsprelated.com/freebooks/filters/

[29] J. Uhlíř and P. Sovka, *Číslicové zpracování signálů.* Praha: Vydavatelství ČVUT, 2002.

[30] T. Oberlin, S. Meignen, and V. Perrier, "The fourier-based synchrosqueezing transform," in *2014 IEEE International Conference on Acoustics, Speech and Signal Processing (ICASSP)*, 2014, pp. 315–319.

Attachments

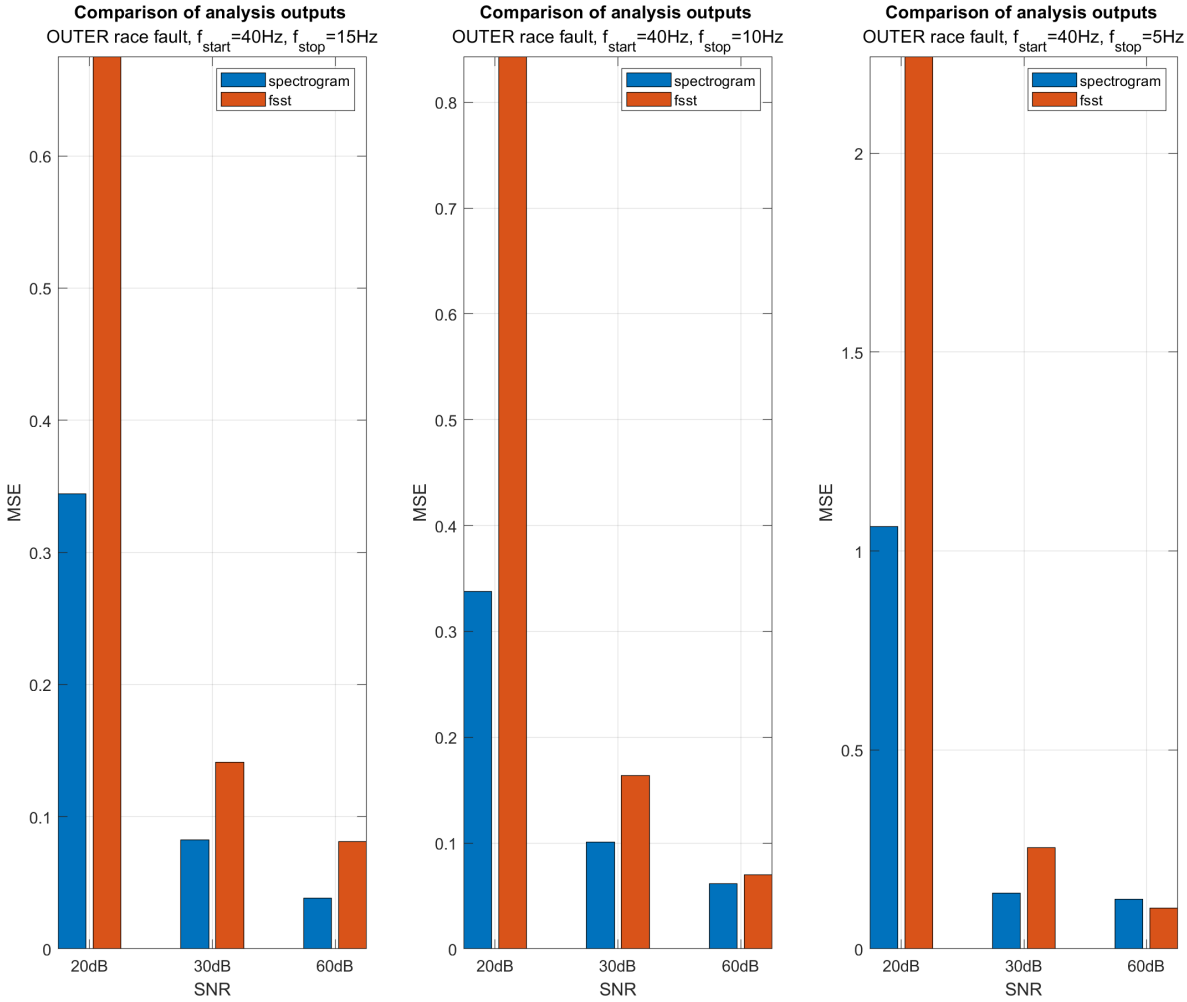

Figure 27: OUTER race fault $f_{start} = 40$ Hz. Comparison of analysis results in order to compare spectrogram and fsstgram methods.

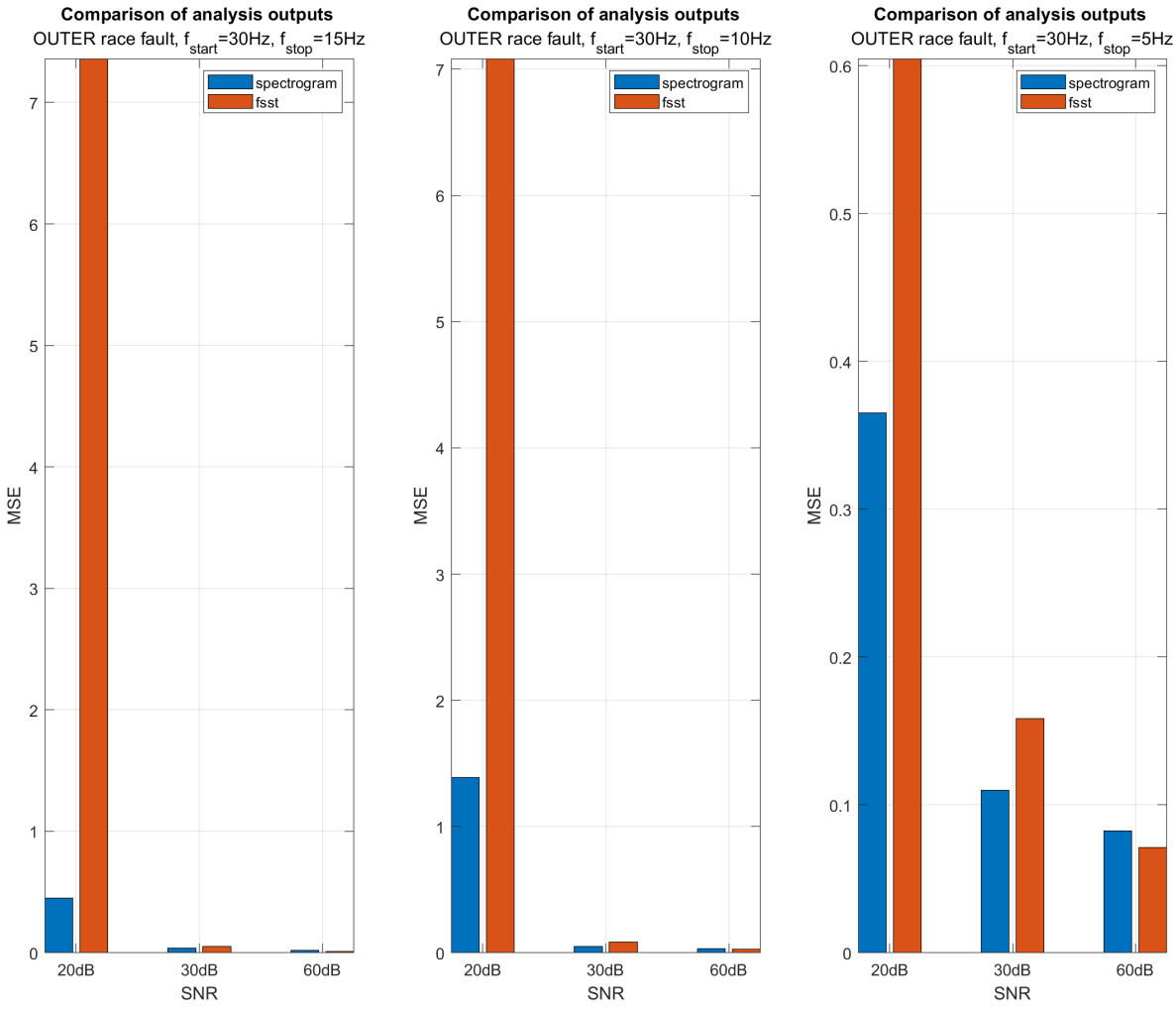

Figure 28: OUTER race fault $f_{start} = 30$ Hz. Comparison of analysis results in order to compare spectrogram and fsstgram methods.

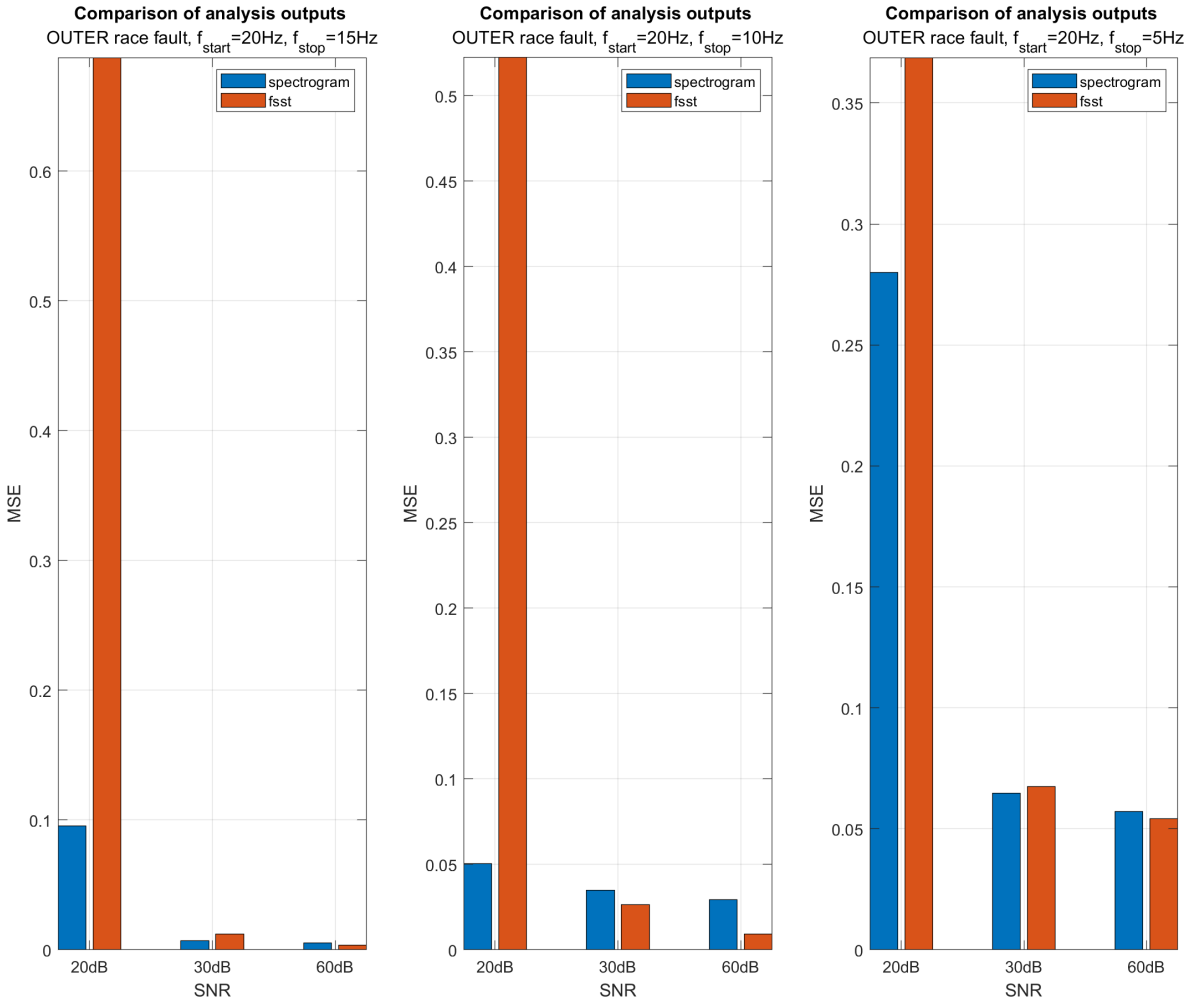

Figure 29: OUTER race fault $f_{start} = 20$ Hz. Comparison of analysis results in order to compare spectrogram and fsstgram methods.

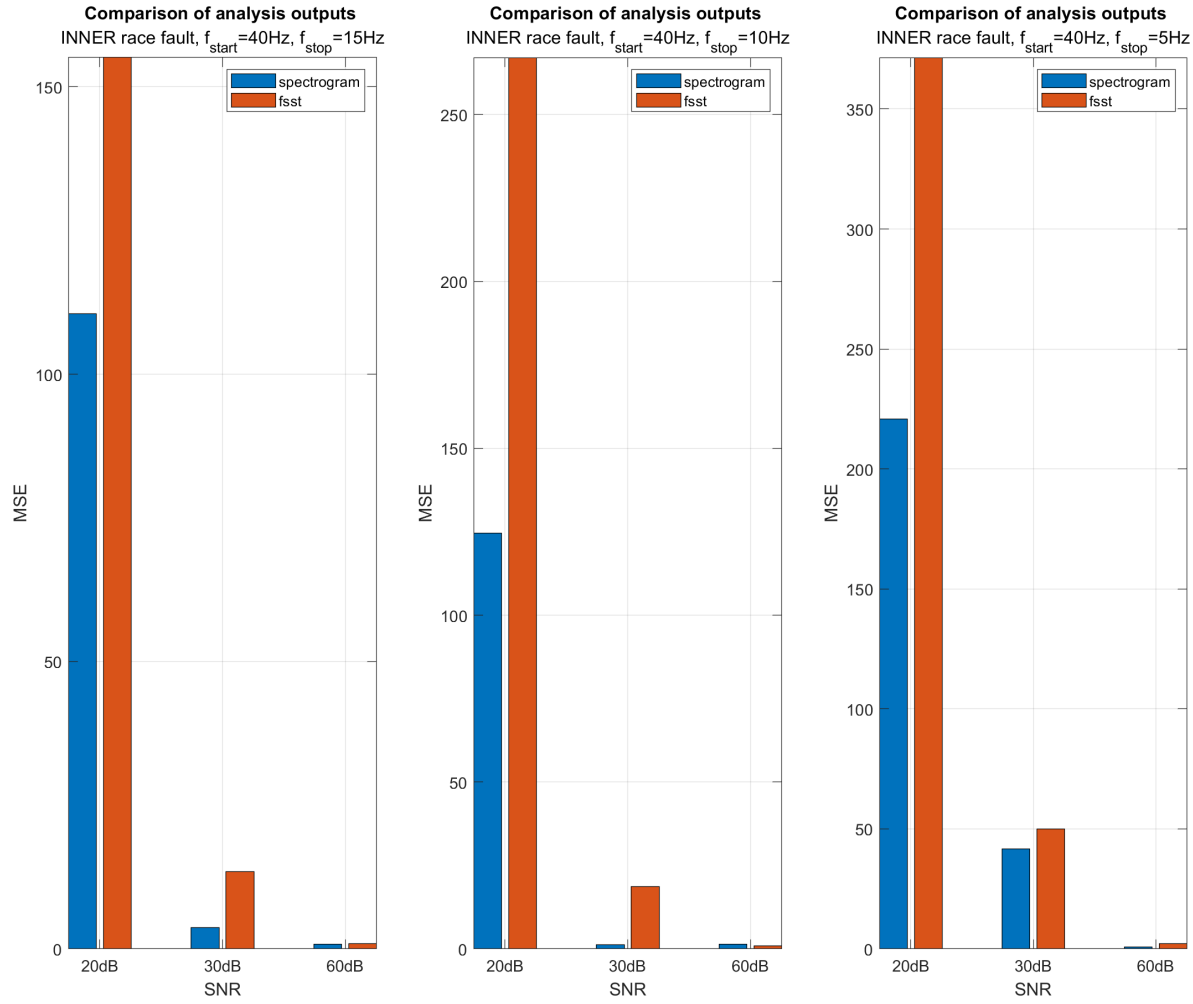

Figure 30: INNER race fault $f_{start} = 40$ Hz. Comparison of analysis results in order to compare spectrogram and fsstgram methods.

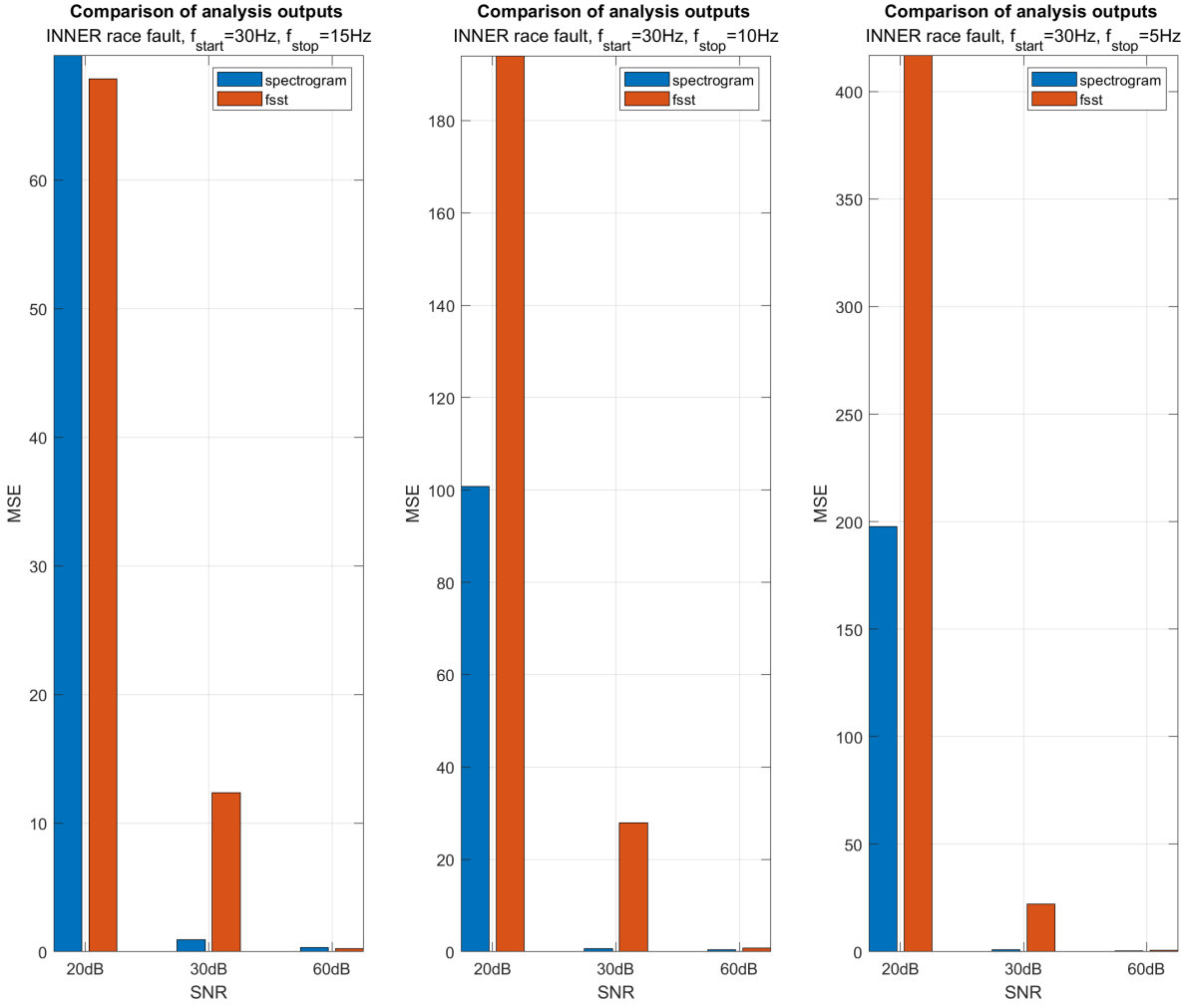

Figure 31: INNER race fault $f_{start} = 30$ Hz. Comparison of analysis results in order to compare spectrogram and fsstgram methods.

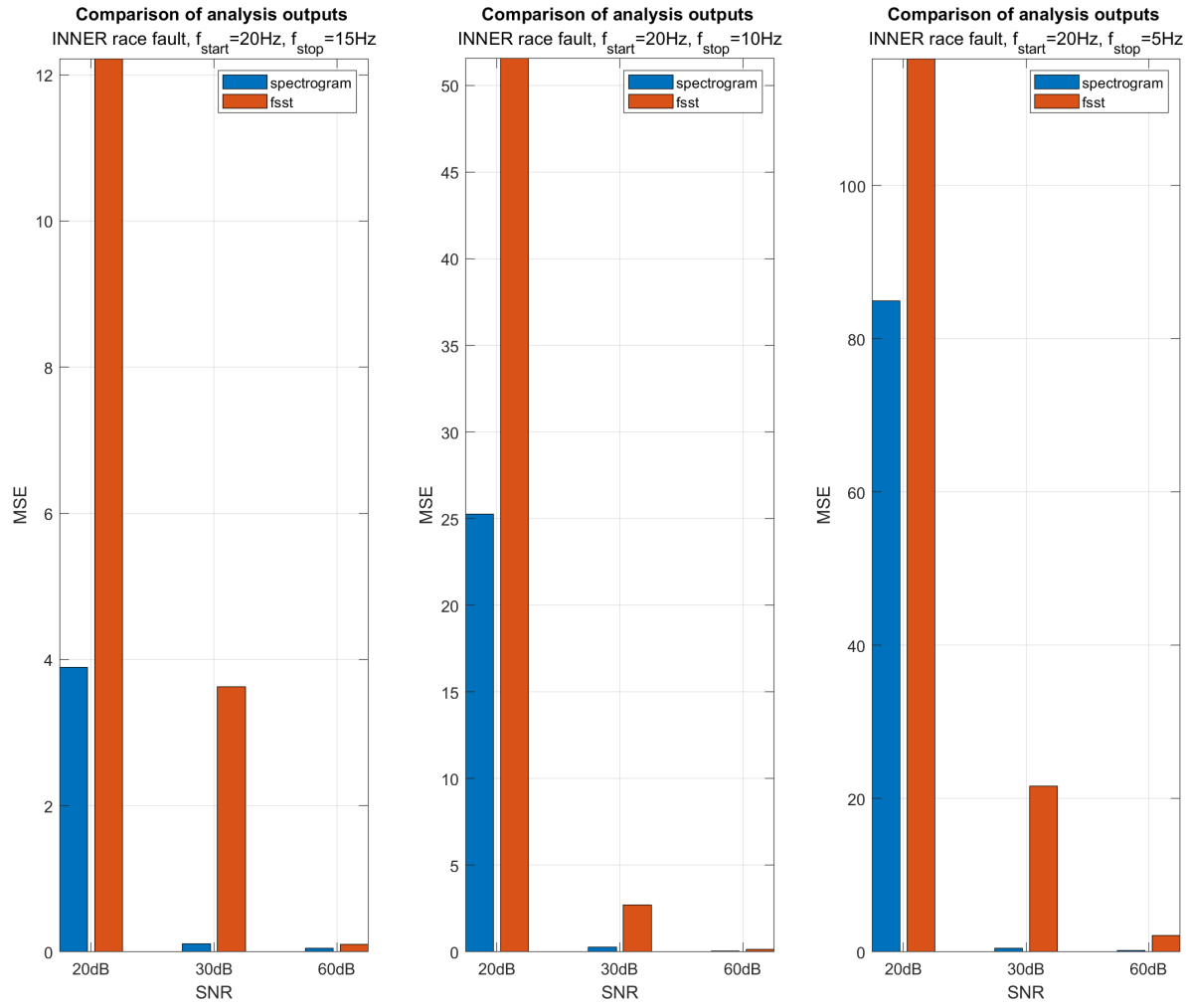

Figure 32: INNER race fault $f_{start} = 20$ Hz. Comparison of analysis results in order to compare spectrogram and fsstgram methods.

File name	Fault type	fstart [Hz]	fstop [Hz]	T [s]	SNR [dB]
OUTER_40Hz_15Hz_3s_60		40	15	3	60
OUTER_40Hz_15Hz_3s_30		40	15	3	30
OUTER_40Hz_15Hz_3s_20		40	15	3	20
OUTER_40Hz_10Hz_3s_60		40	10	3	60
OUTER_40Hz_10Hz_3s_30		40	10	3	30
OUTER_40Hz_10Hz_3s_20		40	10	3	20
OUTER_40Hz_5Hz_3s_60		40	5	3	60
OUTER_40Hz_5Hz_3s_30		40	5	3	30
OUTER_40Hz_5Hz_3s_20		40	5	3	20
OUTER_30Hz_15Hz_3s_60		30	15	3	60
OUTER_30Hz_15Hz_3s_30		30	15	3	30
OUTER_30Hz_15Hz_3s_20		30	15	3	20
OUTER_30Hz_10Hz_3s_60	**OUTER**	30	10	3	60
OUTER_30Hz_10Hz_3s_30	**RACE**	30	10	3	30
OUTER_30Hz_10Hz_3s_20	**FAULT**	30	10	3	20
OUTER_30Hz_5Hz_3s_60		30	5	3	60
OUTER_30Hz_5Hz_3s_30		30	5	3	30
OUTER_30Hz_5Hz_3s_20		30	5	3	20
OUTER_20Hz_15Hz_3s_60		20	15	3	60
OUTER_20Hz_15Hz_3s_30		20	15	3	30
OUTER_20Hz_15Hz_3s_20		20	15	3	20
OUTER_20Hz_10Hz_3s_60		20	10	3	60
OUTER_20Hz_10Hz_3s_30		20	10	3	30
OUTER_20Hz_10Hz_3s_20		20	10	3	20
OUTER_20Hz_5Hz_3s_60		20	5	3	60
OUTER_20Hz_5Hz_3s_30		20	5	3	30
OUTER_20Hz_5Hz_3s_20		20	5	3	20

Table 6.1: The following table describes the generated signal database with the basic descriptive parameters of the signals.

File name	Fault type	fstart [Hz]	fstop [Hz]	T [s]	SNR [dB]
INNER_40Hz_15Hz_3s_60		40	15	3	60
INNER_40Hz_15Hz_3s_30		40	15	3	30
INNER_40Hz_15Hz_3s_20		40	15	3	20
INNER_40Hz_10Hz_3s_60		40	10	3	60
INNER_40Hz_10Hz_3s_30		40	10	3	30
INNER_40Hz_10Hz_3s_20		40	10	3	20
INNER_40Hz_5Hz_3s_60		40	5	3	60
INNER_40Hz_5Hz_3s_30		40	5	3	30
INNER_40Hz_5Hz_3s_20		40	5	3	20
INNER_30Hz_15Hz_3s_60		30	15	3	60
INNER_30Hz_15Hz_3s_30		30	15	3	30
INNER_30Hz_15Hz_3s_20		30	15	3	20
INNER_30Hz_10Hz_3s_60	**INNER**	30	10	3	60
INNER_30Hz_10Hz_3s_30	**RACE**	30	10	3	30
INNER_30Hz_10Hz_3s_20	**FAULT**	30	10	3	20
INNER_30Hz_5Hz_3s_60		30	5	3	60
INNER_30Hz_5Hz_3s_30		30	5	3	30
INNER_30Hz_5Hz_3s_20		30	5	3	20
INNER_20Hz_15Hz_3s_60		20	15	3	60
INNER_20Hz_15Hz_3s_30		20	15	3	30
INNER_20Hz_15Hz_3s_20		20	15	3	20
INNER_20Hz_10Hz_3s_60		20	10	3	60
INNER_20Hz_10Hz_3s_30		20	10	3	30
INNER_20Hz_10Hz_3s_20		20	10	3	20
INNER_20Hz_5Hz_3s_60		20	5	3	60
INNER_20Hz_5Hz_3s_30		20	5	3	30
INNER_20Hz_5Hz_3s_20		20	5	3	20

Table 6.2: The following table describes the generated signal database with the basic descriptive parameters of the signals.